Chapter 3

Theoretical Interpretation of Time-Distance Heliosesismology Data

3.1 Introduction [1]

Time-distance helioseismology, introduced by Duvall et al. (1993b), has yielded numerous exciting results regarding the interior of the Sun. This technique, which gives information about travel times (introduced in section 1.5.2) for wave packets moving between any two points on the solar surface, is an important complement to global-mode helioseismology as it is able to probe subsurface structure and dynamics in three dimensions. Some of the main results concern flows and wave-speed perturbations underneath sunspots (Duvall et al., 1996; Kosovichev & Duvall, 1997; Kosovichev et al., 2000; Zhao et al., 2001), large-scale subsurface poleward flows (Giles et al., 1997; Giles et al., 1998), and supergranulation flows (Duvall et al., 1997; Duvall & Gizon, 2000).

The interpretation of time-distance data can be divided into a forward and an inverse problem. The forward problem is to determine the relationship between

[1] *Parts of the introduction to this chapter are taken from the introductions to three time-distance papers (Birch & Kosovichev, 2000; Birch et al., 2001a; Gizon & Birch, 2002). The three main sections of this chapter are based on published papers; the particulars will be explained at the beginning of each section.*

the observational data (travel-time perturbations $\delta\tau$) and internal solar properties (denoted by q_α). Generally, this relationship is sought in the form of a linear integral equation,

$$\delta\tau = \sum_\alpha \int_\odot \mathrm{d}\boldsymbol{r}\; \delta q_\alpha(\boldsymbol{r})\, K^\alpha(\boldsymbol{r})\,, \tag{3.1}$$

where the $\delta q_\alpha(\boldsymbol{r})$ represent the deviations in internal solar properties from a theoretical reference model. The index α refers to all relevant types of independent perturbations, such as sound speed, flows, or magnetic field. The integral $\int_\odot \mathrm{d}\boldsymbol{r}$ denotes spatial integration over the volume of the Sun. The kernels of the integrals, $K^\alpha(\boldsymbol{r})$, give the sensitivity of travel times to perturbations of the solar model. The inverse problem is to invert the above equation, i.e. to estimate δq_α, as a function of position $\boldsymbol{r}$, from the observed $\delta\tau$. This chapter is concerned only with the forward problem. The inverse problem will be discussed in the first section of Chapter 4.

Accurate computations of the sensitivity of travel times to subsurface conditions are necessary for making quantitative inferences about the Sun from time-distance data. The two approximations that have typically been employed in the modeling of time-distance data, i.e. solving the forward problem, are the ray and single-source approximations.

The ray approximation estimates travel-time perturbations as weighted integrals along the geometrical ray connecting the observation points (Kosovichev, 1996a; D'Silva et al., 1996) and has been employed in the bulk of the time-distance analysis that has been done to date (e.g. Kosovichev & Duvall, 1997; Kosovichev et al., 2000; Chou et al., 2001; Zhao et al., 2001). Ray theory is, however, well known to be inaccurate when applied to structures with sufficiently small length scales, in particular when the length scale of the perturbation is smaller than the first Fresnel zone (e.g. Bogdan & Cally, 1997; Jensen et al., 2000; Hung et al., 2001; Birch et al., 2001a). Efforts to move beyond first order ray theory have focused on the Born approximation (Gizon et al., 2000; Birch & Kosovichev, 2000) and a qualitative Fresnel zone approach (Jensen et al., 1998; Jensen et al., 2001). Both of these approaches are based on previous work in the geophysics literature (e.g. Zhao & Jordan, 1998; Marquering et al., 1999; Dahlen et al., 2000, for the Born approximation) and (e.g. Sneider & Lomax, 1996, for the Fresnel zone approach).

In the single-source approximation the effect of random distributed wave sources

is modeled by a single source at one of the observation points (Jensen et al., 2000; Birch & Kosovichev, 2000). It is known that the main source of waves on the Sun is near-surface convection (e.g. Nigam & Kosovichev, 1999) and as a result the single-source approximation is not an obviously physical approximation. The approximation is, however, motivated by ray theory and by the "Claerbout conjecture": "By cross-correlating noise traces recorded at two locations on the surface, we can construct the wavefield that would be recorded at one of the locations if there was a source at the other." (e.g. Rickett & Claerbout, 1999).

Two studies have emphasized the limitations of the single source approximation. Woodard (1997) employed a distributed-source model to estimate the effect of wave absorption by sunspots on travel times. The effect discovered in that paper cannot easily be modeled in the single-source approximation. Gizon & Birch (2002) showed that travel-time kernels, for surface gravity waves, in the single-source approximation and in a distributed-source model could be qualitatively different. A detailed investigation of the accuracy of the single-source approximation has not yet been done.

This chapter makes three important claims. The first is that ray approximation travel times are inaccurate for perturbations with length scales smaller than the first Fresnel zone. The second is that Born approximation travel times are accurate to lowest order in perturbation strength. The final claim is that the single-source approximation neglects a scattering process and as a result single-source travel-time kernels can be substantially incorrect.

The remainder of this chapter is organized in three sections. The first, section 3.2, employs the Born approximation to compute finite-wavelength travel-time sensitivities in the single-source approximation. In addition, the first section gives a brief numerical comparison between Born and ray approximation travel times. The accuracy of the Born and ray approximations is studied in section 3.3 by comparison with direct numerical solutions of the wave equation. A general Born approximation finite-wavelength distributed-source approach for computing travel-time sensitivities is developed in the final section, 3.4. The final section also shows that single-source and distributed-source kernels, computed for surface-gravity waves, are qualitatively different.

3.2 Single-Source Model for Travel-Time Sensitivities [1]

In this section I will demonstrate the computation of travel-time kernels in the single-source approximation. In this approximation the velocity signal from a single source is taken as a proxy for the cross-correlation function between the "source" and "receiver" points. The "source" point (denoted by the symbol $\mathbf{x}_{\rm s}$) is the location on the solar surface where the source is located and the "receiver" point (denoted by the symbol $\mathbf{x}_{\rm r}$) is where the signal due to the source is observed. In this section the signal is assumed to be radial velocity, which is a good approximation near disk center.

In the single-source approximation the travel-time perturbation is measured from the velocity signal. One possible choice for the definition of travel-time perturbation is

$$d\tau(\mathbf{x}_{\rm s},\mathbf{x}_{\rm r}) = \underset{\tau}{\rm argmax}\left\{ \int_{t_0}^{t_1} {\rm d}t\; v_0(\mathbf{x}_{\rm r},t-\tau)v(\mathbf{x}_{\rm r},t) \right\} . \tag{3.2}$$

The function $\text{argmax}_\tau\,\{f(\tau)\}$ returns the value of τ which maximizes the function $f(\tau)$. Here $v_0(\mathbf{x}_{\rm r},t)$ is the velocity at the receiver in the lowest order solar model, and $v(\mathbf{x}_{\rm r},t)$ is the perturbed velocity at $\mathbf{x}_{\rm r}$. The wave source is located at $\mathbf{x}_{\rm s}$. In equation (3.2), $d\tau(\mathbf{x}_{\rm s},\mathbf{x}_{\rm r})$ depends on $\mathbf{x}_{\rm s}$ as $v(\mathbf{x}_{\rm r},t)$ and $v_0(\mathbf{x}_{\rm r},t)$ are velocity signals due to a source at $\mathbf{x}_{\rm s}$. The time interval $[t_0,t_1]$ should be chosen to isolate the particular part of the velocity signal that is of interest, for example the first-bounce part. From equation (3.2) we see that the travel-time perturbation is the time shift between the unperturbed and perturbed signals at the receiver location, $\mathbf{x}_{\rm r}$. The above definition of travel time and the labels "source" and "receiver" are standard in the geophysics literature (e.g. Zhao & Jordan, 1998).

This section has three main parts. The first (section 3.2.1) is a derivation of travel-time kernels for sound-speed perturbations to a spherical solar model. The second (section 3.2.2) shows that the Born approximation gives the same result as standard normal mode perturbation theory when applied to spherically symmetric

[1] *The material in this section is taken from a Solar Physics paper (Birch & Kosovichev, 2000) and a proceedings paper (Birch & Kosovichev, 2001). I carried out the analytical and numerical calculations, except for the computations of the normal mode eigenfrequencies and eigenfunctions, and wrote the text for both papers.*

perturbations, in an effort to make a connection between time-distance helioseismology and standard global helioseismology. The final section, 3.2.3, shows numerical computations of travel-time kernels and some preliminary comparisons between the ray and Born approximations.

3.2.1 Derivation of Travel-Time Sensitivities

The goal of this section is to compute the travel-time kernels $K(\mathbf{x}_\mathrm{s}, \mathbf{x}_\mathrm{r}; \boldsymbol{r})$ that relate a local perturbation, $\delta c(\boldsymbol{r})$, to the sound speed of the solar model, $c(r)$, to a perturbation to the travel time, denoted by $\delta\tau(\mathbf{x}_\mathrm{s}, \mathbf{x}_\mathrm{r})$, between the two locations $\mathbf{x}_\mathrm{s}$ and $\mathbf{x}_\mathrm{r}$ on the solar surface. The kernels should satisfy

$$\delta\tau(\mathbf{x}_\mathrm{s}, \mathbf{x}_\mathrm{r}) = \int_\odot \mathrm{d}\boldsymbol{r}\, K(\mathbf{x}_\mathrm{s}, \mathbf{x}_\mathrm{r}; \boldsymbol{r}) \frac{\delta c^2(\boldsymbol{r})}{c^2(r)}. \tag{3.3}$$

The integral $\int_\odot \mathrm{d}\boldsymbol{r}$ means integration over the entire volume of the sun.

The first step in the derivation of kernels is to compute the radial velocities v_0 and v in the unperturbed and perturbed solar models, respectively. A linear relation between travel-time perturbations and perturbations to the solar model, in the form of equation (3.3), can then be obtained by linearizing equation (3.2). The remainder of this section, 3.2.1, completes this task.

Governing Equations

The standard equation of motion (e.g. Gough, 1987) in the Cowling approximation, for the fluid displacement field $\boldsymbol{\xi}$ due to a source $\boldsymbol{S}$, is

$$\left(\rho\partial_t^2 + \mathcal{L}\right)\boldsymbol{\xi} = \boldsymbol{S}\,, \tag{3.4}$$

where ρ is the density and $\mathcal{L}$ is the spatial part of the wave equation operator. Here the function $\boldsymbol{S}$ represents an impulsive monopole source, which we take as

$$\boldsymbol{S} = A\boldsymbol{\nabla}\delta_D(\mathbf{x} - \mathbf{x}_\mathrm{s})\delta_D(t - t_s)\,, \tag{3.5}$$

where $\mathbf{x}_s$ is the source location, t_s is the time of the impulse, A gives the amplitude of the source, δ_D is the Dirac delta function, and $\boldsymbol{\nabla}$ is the gradient with respect to the variable $\mathbf{x}$.

In order to apply the Born approximation we split the problem into the unperturbed (subscript 0) and first-order correction (preceded by a δ) parts. In general we expect that the perturbation to the travel time should depend on the perturbations to density and sound speed and as in the case of global helioseismology both kernels are needed in order to do inversions. In this work, in order to demonstrate the general approach, we calculate only the sensitivity of travel times to perturbations to sound speed at fixed density. The problem can thus be written as

$$\left(\rho_0\partial_t^2 + \mathcal{L}_0 + \delta\mathcal{L}\right)\left(\boldsymbol{\xi}_0 + \delta\boldsymbol{\xi}\right) = A\boldsymbol{\nabla}\delta_D(x - \mathbf{x}_s)\delta_D(t - t_s)\,. \tag{3.6}$$

The unperturbed and perturbed operators $\mathcal{L}^0$ and $\delta\mathcal{L}$ are

$$\mathcal{L}_0\boldsymbol{\xi} = \boldsymbol{\nabla}\left[c_0^2\rho_0\boldsymbol{\nabla}\cdot\boldsymbol{\xi} - \xi_r\frac{dP_0}{dr}\right] - \mathbf{g}_0\boldsymbol{\nabla}\cdot\left(\rho_0\boldsymbol{\xi}\right), \tag{3.7}$$

$$\delta\mathcal{L}\boldsymbol{\xi} = \boldsymbol{\nabla}\left[\delta c^2\rho_0\boldsymbol{\nabla}\cdot\boldsymbol{\xi}\right], \tag{3.8}$$

where c_0 is the adiabatic sound speed, $\mathbf{g}_0$ is the gravitational acceleration (which is a function of depth), P_0 is the gas pressure, and δc is the perturbation to the sound speed, which in general is non-spherical. The radial component of $\boldsymbol{\xi}$ is denoted by ξ_r.

The lowest order problem is

$$(\rho_0\partial_t^2 + \mathcal{L}_0)\boldsymbol{\xi}_0 = A\boldsymbol{\nabla}\delta_D(x - x_0)\delta_D(t - t_s)\,, \tag{3.9}$$

and the first-order problem is

$$(\rho_0\partial_t^2 + \mathcal{L}_0)\delta\boldsymbol{\xi} = -\delta\mathcal{L}\boldsymbol{\xi}_0\,. \tag{3.10}$$

Solution of the Lowest Order Problem

For the spherically symmetric case the eigenfunctions and eigenvalues of the operator $(\rho\partial_t^2 + \mathcal{L}_0)$ are well known (e.g. Gough, 1987). We use the standard convention of

labeling the radial order by n, the angular degree by l, and the azimuthal order by m. For the normalization of the eigenfunctions we choose

$$\int_{\odot} \mathrm{d}\boldsymbol{r}\ \rho_0(r)\boldsymbol{\xi}^{nlm}(\boldsymbol{r}) \cdot \boldsymbol{\xi}^{nlm}(\boldsymbol{r}) = 1\,. \tag{3.11}$$

For convenience of notation, following the approach of Dahlen & Tromp (1998) we represent the unperturbed eigenfunctions in terms of the real vector spherical harmonics $\mathbf{P}_{lm}$ and $\mathbf{B}_{lm}$

$$\boldsymbol{\xi}^{nlm}(r,\theta,\phi) = \xi_r^{nl}(r)\mathbf{P}_{lm}(\theta,\phi) + \xi_h^{nl}(r)\mathbf{B}_{lm}(\theta,\phi)\,, \tag{3.12}$$

where ξ_h^{nl} and ξ_h^{nl} are the radial and horizontal components of the displacement. The vector spherical harmonics can be written in terms of the real (scalar) spherical harmonics, $Y_{lm}(\theta,\phi)$, as

$$\mathbf{P}_{lm}(\theta,\phi) = \hat{\mathbf{r}}Y_{lm}(\theta,\phi)\,, \tag{3.13}$$

$$\mathbf{B}_{lm}(\theta,\phi) = \frac{1}{\sqrt{l(l+1)}}\boldsymbol{\nabla}_1 Y_{lm}(\theta,\phi)\,, \tag{3.14}$$

where $\boldsymbol{\nabla}_1$ is the horizontal gradient on the unit sphere (Dahlen & Tromp, 1998).

The solution to the zero-order problem is then obtained as the sum of the eigenfunctions. For the radial component of the oscillation velocity at a location $\mathbf{x}_1$ at time t due to a source at time $t_s = 0$ and location $\mathbf{x}_0$ we obtain

$$v_0(\Delta,t) = -A\sum_{n=0}^{\infty}\sum_{l=0}^{\infty}\frac{2l+1}{4\pi}D^{nl}(R_\odot)\xi_r^{nl}(R_\odot)P_l(\cos\Delta)\mathrm{Hea}(t)\cos(\omega_{nl}t) \tag{3.15}$$

where we have assumed that the source and observation points $\mathbf{x}_\mathrm{s}$ and $\mathbf{x}_\mathrm{r}$ are on the solar surface, that the displacement field is zero at time zero, and that the solar surface is free. The great circle distance between $\mathbf{x}_\mathrm{s}$ and $\mathbf{x}_\mathrm{r}$ is denoted by Δ. The P_l are the Legendre polynomials, Hea the Heaviside function, and

$$D^{nl} = \frac{d\xi_r^{nl}}{dr} + \frac{1}{r}\left[2\xi_r^{nl} - \sqrt{l(l+1)}\xi_h^{nl}\right]\,, \tag{3.16}$$

which comes from taking the divergence of the eigenfunctions. Notice that the zero order velocity signal depends only on the great circle distance between $\mathbf{x}_\mathrm{s}$ and $\mathbf{x}_\mathrm{r}$

and the time t.

First Born Approximation

We recall that the first-order problem is

$$(\rho\partial_t^2 + \boldsymbol{\mathcal{L}})\delta\boldsymbol{\xi} = -\delta\boldsymbol{\mathcal{L}}\boldsymbol{\xi}_0\,, \tag{3.17}$$

with $\boldsymbol{\xi}_0$ the solution to the unperturbed problem. The operator on the left hand side of the equation is the same as for the zero-order problem and thus we can solve the first-order problem in exactly the same manner as we did the unperturbed problem.

The first-order solution for the radial velocity is then

$$\begin{aligned}\delta v(\mathbf{x}_\mathrm{s}, \mathbf{x}_\mathrm{r}, t) &= A\int_\odot \mathrm{d}\boldsymbol{r}\ \rho_0(r)\delta c^2(\boldsymbol{r})\mathrm{Hea}(t) \\ &\quad\times \sum_{n,n'=0}^{\infty}\sum_{l,l'=0}^{\infty} S_{nl}(\mathbf{x}_\mathrm{s},\boldsymbol{r})R_{n'l'}(\mathbf{x}_\mathrm{r},\boldsymbol{r})\frac{\cos(\omega_{nl}t)-\cos(\omega_{n'l'}t)}{\omega_{n'l'}^2-\omega_{nl}^2}\,,\end{aligned} \tag{3.18}$$

where

$$S_{nl}(\mathbf{x}_\mathrm{s},\boldsymbol{r}) = \frac{2l+1}{4\pi}D^{nl}(R_\odot)D^{nl}(r)P_l(\cos\Delta_1)\,, \tag{3.19}$$

$$R_{nl}(\mathbf{x}_\mathrm{r},\boldsymbol{r}) = \frac{2l+1}{4\pi}\xi_r^{nl}(R_\odot)D^{nl}(r)P_l(\cos\Delta_2)\,. \tag{3.20}$$

The great-circle distance between $\mathbf{x}_\mathrm{s}$ ($\mathbf{x}_\mathrm{r}$) and $\boldsymbol{r}$ is denoted by Δ_1 (Δ_2).

Kernels

Now that we have the unperturbed and the first Born approximation responses, v_0 and $v_0+\delta v$ respectively, we can calculate the time lag between them. The linearization of the dependence of $\delta\tau$ on δv in equation (3.2) gives, with the assumption that the time window $[t_0, t_1]$ isolates a particular bounce in the cross-correlation,

$$\delta\tau = \frac{1}{N(\Delta)}\int_{t_0}^{t_1}\mathrm{d}t\ \dot{v}_0(t)\delta v(t) \tag{3.21}$$

with

$$N(\Delta) = \int_{t_0}^{t_1} \mathrm{d}t\ \ddot{v}_0(\Delta, t) v_0(\Delta, t)\,. \tag{3.22}$$

By plugging equation (3.18) into equation (3.21) we obtain

$$\begin{aligned} \delta\tau &= \frac{A}{N(\Delta)} \int_{\odot} \mathrm{d}\boldsymbol{r}\ \rho_0(r) c^2(r) \frac{\delta c^2(\boldsymbol{r})}{c^2(r)} \sum_{n,n'=0}^{\infty} \sum_{l,l'=0}^{\infty} \\ &\quad \times S_{nl}(\mathbf{x}_\mathrm{s}, \boldsymbol{r}) R_{n'l'}(\mathbf{x}_\mathrm{r}, \boldsymbol{r}) \int_{t_0}^{t_1} \mathrm{d}t\ \dot{v}_0(\Delta, t) \frac{\cos(\omega_{nl} t) - \cos(\omega_{n'l'} t)}{\omega_{nl}^2 - \omega_{n'l'}^2}\,. \end{aligned} \tag{3.23}$$

It is convenient to obtain kernels for the fractional perturbation to the square of the sound speed, which satisfy equation (3.3). From equation (3.23) we can see then that

$$\begin{aligned} K(\mathbf{x}_\mathrm{s}, \mathbf{x}_\mathrm{r}\ \boldsymbol{r}) &= \frac{-A}{N(\Delta)} \rho_0(r) c^2(r) \sum_{n,n'=0}^{\infty} \sum_{l,l'=0}^{\infty} \\ &\quad \times S_{nl}(\mathbf{x}_\mathrm{s}, \boldsymbol{r}) R_{n'l'}(\mathbf{x}_\mathrm{r}, \boldsymbol{r}) \int_{t_0}^{t_1} \mathrm{d}t\ \dot{v}_0(\Delta, t) \frac{\cos(\omega_{nl} t) - \cos(\omega_{n'l'} t)}{\omega_{nl}^2 - \omega_{n'l'}^2}\,. \end{aligned} \tag{3.24}$$

This equation can be simplified by introducing the collective indices $p = (n, l)$ and $q = (n', l')$ and defining the matrix

$$G_{pq}(\mathbf{x}_\mathrm{s}, \mathbf{x}_\mathrm{r}) = \frac{A}{N(\Delta)} \int_{t_0}^{t_1} dt\ \dot{v}_0(\Delta, t) \frac{\cos(\omega_p t) - \cos(\omega_q t)}{\omega_p^2 - \omega_q^2}\,. \tag{3.25}$$

Notice that $N \propto A^2$ and $v_0 \propto A$ so that the matrix $\mathbf{G}$ does not depend on A, the amplitude of the source. With the above definitions the kernel can then be written as

$$K(\mathbf{x}_\mathrm{s}, \mathbf{x}_\mathrm{r}, \boldsymbol{r}) = -\rho_0(r) c_0^2(r) \mathbf{S}^T(\mathbf{x}_\mathrm{s}, \boldsymbol{r}) \mathbf{G}(\mathbf{x}_\mathrm{s}, \mathbf{x}_\mathrm{r}) \mathbf{R}(\mathbf{x}_\mathrm{r}, \boldsymbol{r}) \tag{3.26}$$

where the superscript T denotes the transpose.

Note that the kernels $K(\mathbf{x}_\mathrm{s}, \mathbf{x}_\mathrm{r}; \boldsymbol{r})$ are not, however, symmetric on interchange of the source and the receiver locations, $\mathbf{x}_\mathrm{s}$ and $\mathbf{x}_\mathrm{r}$. The asymmetry is a result of the single-source model, in which modes that have large divergence at the source are most excited and modes which have the largest radial velocities at the surface contribute most strongly to the observed signal. Since there is no isolated point

source on the Sun, in reality travel times are determined from a cross-covariance function. The exact relationship between the single-source model and the physical distributed-source model is not established yet. For discussions of the problem see (Rickett & Claerbout, 2000; Kosovichev et al., 2000) as well as the final section of this chapter. Therefore, in order to obtain the desired symmetry, we simply replace the divergence and vertical displacement at the solar surface that appear in the vectors $\mathbf{S}$ and $\mathbf{R}$ with the square root of some function F^{nl}. The square root is used so that the zero-order velocity is

$$v_0(\Delta, t) = -A \sum_{n=0}^{\infty} \sum_{l=0}^{\infty} \frac{2l+1}{4\pi} F^{nl}(R_\odot) P_l(\cos\Delta) \mathrm{Hea}(t) \cos(\omega_{nl} t) \,. \tag{3.27}$$

The function F^{nl} is the amplitude with which each mode contributes to the zero-order velocity signal and is thus related to the filtering that is done to the data in the process of making a time-distance measurement (Kosovichev & Duvall, 1997). The above equation for v_0, with the Heaviside function removed, is essentially equation (9) for the cross-correlation from Kosovichev & Duvall (1997), which is further justification for the substitution of $\sqrt{F^{nl}}$ for the divergence and radial velocities at the solar surface.

We replace the vectors $\mathbf{S}$ and $\mathbf{R}$ with a vector $\mathbf{H}$, defined as

$$H_{nl}(\boldsymbol{r}', \boldsymbol{r}) = \frac{2l+1}{4\pi} \sqrt{F^{nl}} D^{nl}(r) P_l(\cos\Delta') \,, \tag{3.28}$$

where Δ' is the great circle distance between $\boldsymbol{r}'$ and $\boldsymbol{r}$. In terms of $\mathbf{H}$ the travel-time sensitivity kernels in the first Born approximation are

$$K(\mathbf{x}_\mathrm{s}, \mathbf{x}_\mathrm{r}\, \boldsymbol{r}) = -\rho_0(r) c_0^2(r) \mathbf{H}^T(\mathbf{x}_\mathrm{s}, \boldsymbol{r}) \mathbf{G}(\mathbf{x}_\mathrm{s}, \mathbf{x}_\mathrm{r}) \mathbf{H}(\mathbf{x}_\mathrm{r}, \boldsymbol{r}) \,. \tag{3.29}$$

We now have travel-time sensitivity kernels, for sound speed, in the single-source approximation. This result was obtained through straightforward application of the Born approximation and a linearization of the definition of travel time. The essential physical argument was that the velocity from a single source behaves in the same way as the time-distance correlation function. Later in this chapter I will show that this assumption is not entirely correct.

3.2.2 The Born Approximation and Normal Mode Coupling

This section is an attempt to elaborate further on the use of the Born approximation to understand the relationship between time-distance measurements and sound-speed perturbations. We will restrict our attention, for the sake of computational and conceptual simplicity, to sound-speed perturbations that are constant on shells of constant radius. For this case, we will show that the Born approximation is the same as standard first order normal mode perturbation theory.

As we showed in the previous section (eq. [3.15]), the radial velocity resulting from a unit impulsive monopole source at the solar surface is

$$v_0(\Delta,t)=\sum_{n=0}^{\infty}\sum_{l=0}^{\infty}\frac{2l+1}{4\pi}\xi_r^{nl}(R_\odot)D^{nl}(R_\odot)P_l(\cos\Delta)\mathrm{Hea}(t)\cos\omega_{nl}t \tag{3.30}$$

where Δ is the great circle distance between source and receiver, P_l are the Legendre polynomials, $\boldsymbol{\nabla}\cdot\boldsymbol{\xi}^{nlm}(r,\theta,\phi)=D^{nl}(r)Y_{lm}(\theta,\phi)$, and we have adopted $A=-1$ for convenience. The Y_{lm} are real spherical harmonics (Dahlen & Tromp, 1998). Equation (3.30) is exact only if the eigenfunctions form a complete basis.

We want to obtain the first order correction to the velocity that results from a change in the sound speed, assuming that the change in sound speed depends on radius only. This can be done by computing the first order corrections to the functions $\xi_r^{nl}(R_\odot)$, $D^{nl}(R_\odot)$, and the normal mode frequencies ω_{nl}.

The frequencies and eigenfunctions of the normal modes of the Sun can be can be obtained from equation (3.4) by assuming harmonic time dependence for the displacement field $\boldsymbol{\xi}$ and putting the source function $\boldsymbol{S}$ equal to zero. The result is

$$\frac{1}{\rho}\boldsymbol{\mathcal{L}}\boldsymbol{\xi}=\omega^2\boldsymbol{\xi}\,. \tag{3.31}$$

The boundary conditions are regularity at the center of the Sun and zero Lagrangian pressure perturbation at the outer boundary.

We then add a perturbation to the sound speed in the solar model; this corresponds to adding a perturbation $\delta\boldsymbol{\mathcal{L}}$ with

$$\delta\boldsymbol{\mathcal{L}}\boldsymbol{\xi}=-\boldsymbol{\nabla}\left[\rho\,\delta c^2\boldsymbol{\nabla}\cdot\boldsymbol{\xi}\right]\,, \tag{3.32}$$

to the operator $\mathcal{L}$ in equation (3.31). The perturbations to the frequencies and eigenfunctions can be found in the standard way (e.g. Sakurai, 1995)

$$\delta\omega_{nl}^2 = \delta\mathcal{L}_{nn}^l \,, \tag{3.33}$$

$$\delta\boldsymbol{\xi}^{nl} = \sum_{n',n'\neq n} \frac{\delta\mathcal{L}_{nn'}^l}{\omega_{nl}^2 - \omega_{n'l}^2}\boldsymbol{\xi}^{n'l} \,, \tag{3.34}$$

with

$$\delta\mathcal{L}_{nn'}^l = \int_0^{R_\odot} \rho r^2 \mathrm{d}r \; \delta c^2(r) D^{nl}(r) D^{n'l}(r) \,. \tag{3.35}$$

The first order correction to the velocity signal is obtained by employing the perturbations to ω and $\boldsymbol{\xi}$ from equations (3.33) and (3.34) to make the first order corrections to v^0 in equation (3.30). The result is

$$\begin{aligned} \delta v = & \sum_{l=0}^{\infty}\sum_{n,n'=0}^{\infty} \frac{2l+1}{4\pi}\xi_r^{nl}(R_\odot) D^{n'l}(R_\odot) P_l(\cos\Delta) \\ & \times \frac{\cos(\omega_{nl}t) - \cos(\omega_{n'l}t)}{\omega_{nl}^2 - \omega_{n'l}^2} \\ & \times \int_0^{R_\odot} \rho r^2 \mathrm{d}r \; \delta c^2(r) D^{nl}(r) D^{n'l}(r) \,, \end{aligned} \tag{3.36}$$

with the understanding that the $n = n'$ terms are replaced with the limit $\omega_{nl} \to \omega_{n'l}$. So far we have only used standard normal-mode perturbation theory. The above result is, however, exactly the Born approximation result (eq. [3.18]) once the integration over latitude and longitude has been done in that equation.

Notice that equation (3.36) is essentially a sum over pairs of coupled normal modes. As the perturbation is spherically symmetric, modes of different angular degree l are not coupled. The result that in the case of spherically symmetric sound-speed perturbations the Born approximation and normal-mode perturbation theory are identical is perhaps not surprising, as both should be correct to first order. This result, however, does give us some confidence in the Born approximation. Helioseismologists are very comfortable with normal perturbation theory, and this result provides some connection between standard global mode helioseismology and time-distance helioseismology.

3.2.3 Numerical Examples

In this section I will show the results of a numerical computation of a three-dimensional travel-time kernel for local perturbations to sound speed, equation (3.29). I will then show a comparison between one-dimensional ray and Born approximation travel-time kernels for spherically symmetric sound-speed perturbations. Finally a brief comparison will be made between forward calculations in the ray and Born approximations.

Three-Dimensional Born Approximation Kernels

The goal of this subsection is not to give a complete catalog of travel-time kernels but rather to give a single simple example. Figure 3.1 shows slices through a Born approximation sensitivity kernel, for the first-bounce travel time at a heliocentric distance of 22.5° between source and receiver. The source and receiver are located at the surface beneath the $-11.2°$ and 11.2° labels in the left hand panel. The color scale shows the value of the kernel multiplied by the sound speed in the background model. The ray path, computed for a 5.2 minute wave packet, is shown by the black line. For this example calculation, I used a filter function F^{nl} that is Gaussian in frequency, centered at 3.2 mHz with a HWHM of 0.56 mHz. 6000 normal modes were used in the (implicit) double sum in equation (3.29).

Figure 3.1 shows that travel times are indeed sensitive to sound-speed perturbations that are not located on the ray path. This is certainly not a surprise. Secondly, we see that the kernel is not even maximum along the ray path, but rather on a hollow tube around the ray path. This is a result that is particular to working in three spatial dimensions. In two dimensions, for example, travel-time kernels are maximum along the ray path. Finally, we see that the sensitivity of travel times to sound-speed perturbations oscillates with distance from the ray path. The rate of oscillation is controlled by the central frequency of the filter, and the decay rate of the oscillations by the frequency width of the filter. None of these results are fundamentally new; these kernels, dubbed "banana-doughnut" kernels, have been studied in the geophysics literature for the case of wave propagation in the earth (e.g. Marquering et al., 1999).

The computational burden for obtaining these kernels is substantial. Each of

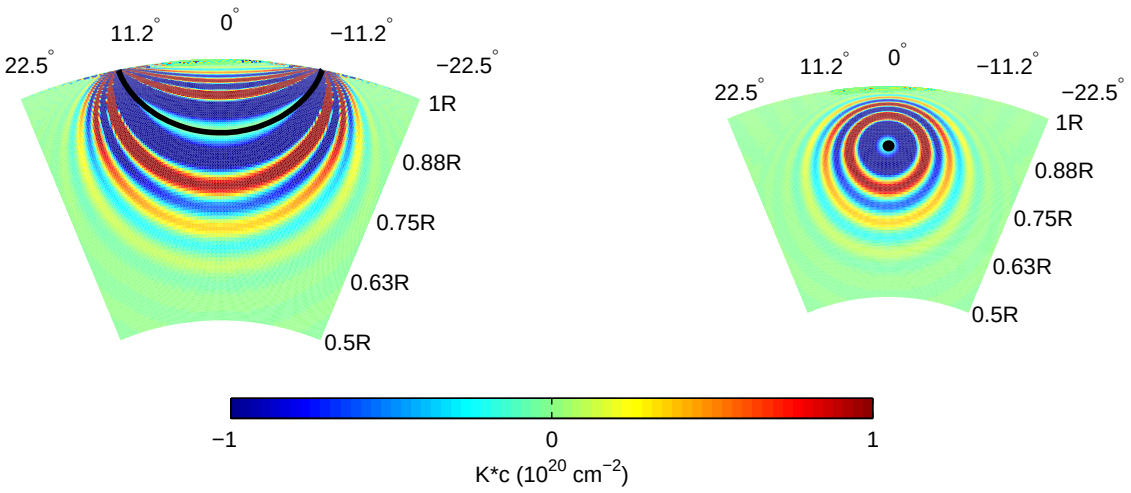

Figure 3.1: Slices through a travel-time kernel, in the source-receiver great-circle plane (left panel) and perpendicular to the ray path at the lower turning point (right panel), multiplied by the background sound speed. The source and receiver are located on the surface at the $-11.2°$ and $11.2°$ marks respectively, in the left hand panel. The color scale does not indicate the full range of variation of the value of the kernel; it is truncated in order to show the details. The black line connecting the source to the receiver is the ray path calculated for a wave packet with a central period of 5.2 minutes. This kernel was calculated using 6000 p modes with $l < 1000$ and the filter function F^{nl} Gaussian in frequency with a central frequency of 3.2 mHz and FWHM of 0.56 mHz.

the two dimensional slices computed here took 8 hours on a 2 GHz Pentium IV, although the code was written in MATLAB and not at all optimized. A. Kosovichev rewrote the code in FORTRAN and saw only a minor improvement. We have not yet seriously investigated the problem of how to speed up the calculations.

Comparison of One-Dimensional Born and Ray Kernels

Travel-time kernels for sound speed can also be derived in the ray approximation (e.g. Kosovichev & Duvall, 1997). For the spherically symmetric case they can be written

$$K_{\rm ray}(r) = -\left(1 + \frac{\omega_c^2}{\omega^2 - \omega_c^2}\right) \frac{dt_\phi(r)}{dr} \tag{3.37}$$

where ω_c is the acoustic cut-off frequency, ω is the frequency, in this case 3.2 mHz, and $t_\phi(r)$ measures the phase time along the ray as a function of radius. Notice that the ray kernels are singular at the lower turning point as a result of the derivative of the phase time.

A comparison of the ray and Born kernels, for a distance of 22.5°, is shown in Figure 3.2. The Born approximation kernel was computed by using the normal mode coupling approach for $\delta \boldsymbol{v}$ (eq. [3.36]) and the machinery of section 3.2.1. The filter function is the same as in the previous subsection, i.e. Gaussian centered at 3.2 mHz with a HWHM of 0.56 mHz. Again 6000 normal modes were used in the calculation. The ray and Born kernels are of the same order of magnitude and essentially of the same sign, i.e. increases in sound speed give decreases in travel time. Notice that the ray kernel is identically zero below the lower turning point of the ray. In contrast, as we saw in Figure 3.1, the Born approximation kernel has weight below the ray path. The ray kernel is singular at the lower turning point, while the Born approximation kernel is finite.

In order to make a further comparison between the ray and Born approximations, we made a series of forward calculations, i.e. calculations of travel-time perturbations due to known sound-speed perturbations. The result of these forward calculations is shown in Figure 3.3. For perturbations with large spatial scale (left panel) the Born and ray approximations agree. In the right panel the spatial scale of the sound-speed perturbation is reduced by a factor of ten and the two approximations give quite different results. In particular, the ray approximation gives zero

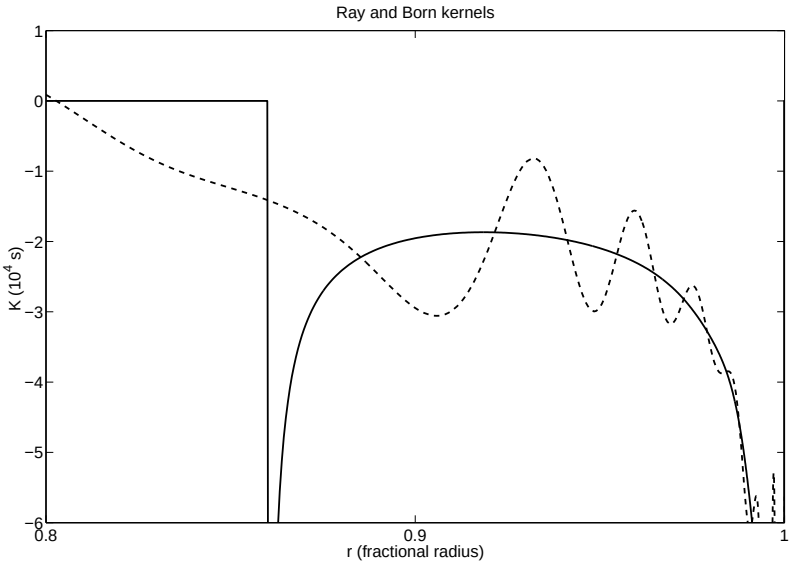

Figure 3.2: A comparison of one-dimensional ray and Born kernels (obtained by assuming the perturbation to the sound speed depends only on radius). Note that the ray kernel is singular at the lower turning point while the Born kernel is finite. The vertical axis is truncated and does not show the full range of variation of the kernels near the surface. The ray kernel is for a frequency of 3.2 mHz. The Born approximation kernel is computed from 6000 normal modes, with a filter that is Gaussian, with a central frequency of 3.2 mHz and HWHM of 0.56 mHz. These kernels are for a perturbation to the sound speed (not the square of the sound speed).

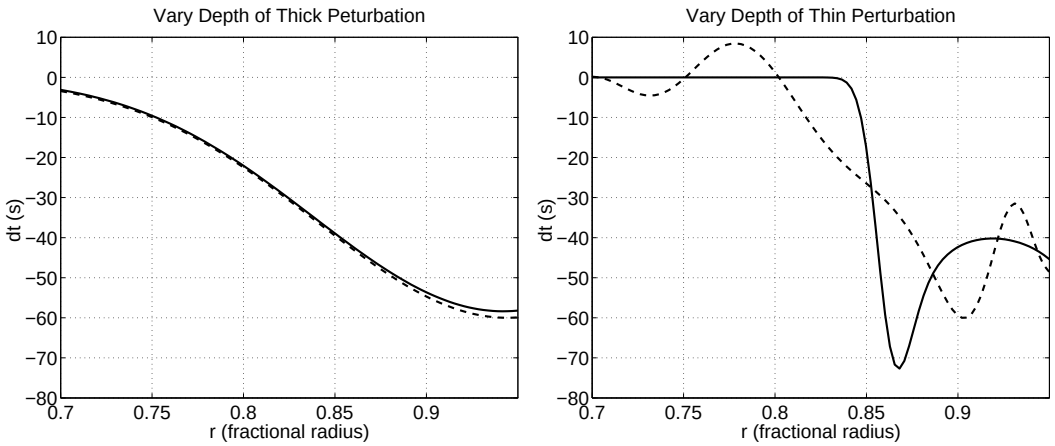

Figure 3.3: Travel-time perturbations due to sound-speed perturbations in the ray (solid line) and Born (dashed line) approximations. The left panel is for sound-speed perturbations with Gaussian dependence on radius, with amplitude of 1.6%, FWHM of $0.2R_\odot$, and varying central radius, r. In the right panel the FWHM is reduced to $0.02R_\odot$ and the amplitude increased to 10%. The calculations were done using the kernels shown in Figure 3.2.

when the sound-speed perturbation is located below the lower turning point, as we saw in Figure 3.2. Even above the turning point, the two approximations can differ by a factor of two for the thin sound-speed perturbation (right panel)

3.3 The Accuracy of the Born and Ray Approximations[1]

In this section we address, by comparison with exact numerical results, the issue of the validity of the Born approximation, which is a finite-wavelength single-scattering approximation (e.g. Sakurai, 1995), in combination with the linearization of the dependence of travel time on the perturbed waveform. We also study the accuracy of the first-order ray approximation. We work with the same model as Hung et al. (2000) but with parameters and source function appropriate to time-distance helioseismology rather than terrestrial seismology. The model is very idealized: adiabatic

[1] *This taken from an ApJ paper (Birch, Kosovichev, Price, & Schlottman, 2001). I did the Born and ray approximation calculations and wrote the text of the paper. G. Price did the numerical work for the uniform sphere cases. I ran the finite difference code, provided by B. Schlottman, for the smooth sphere cases.*

acoustic wave propagation in a three dimensional homogeneous background medium with sound-speed perturbations that are constant on spheres. While very simplistic, the model does allow a relatively straightforward investigation of the ability of the Born and ray approximations to capture the effect of localized sound-speed inhomogeneity on acoustic waves.

We study the scattering of acoustic waves, in three dimensions, from a spherical region where the sound speed differs from the background sound speed; this is the same problem studied by Hung et al. (2000) and Hung et al. (2001). The pressure fluctuations, $p(\boldsymbol{x}, t)$, associated with the acoustic wave are governed by the standard wave equation,

$$\left\{ \frac{\partial^2}{\partial t^2} - c^2(\boldsymbol{x}) \nabla^2 \right\} p(\boldsymbol{x}, t) = w(t) \delta(\boldsymbol{x} - \boldsymbol{x}_s), \tag{3.38}$$

where $c^2(\boldsymbol{x})$ is the square of sound speed, $w(t)$ the source function, and $\boldsymbol{x}_s$ the source location. We use

$$w(t) = \exp\left(-at^2\right) \cos\left(\omega_0 t\right) \tag{3.39}$$

with $\omega_0/2\pi = 3$ mHz and $a = 4 \times 10^{-6}$ s^{-2}, corresponding to a solar-like FWHM of the power spectrum of 0.75 mHz. The background medium has a sound speed of $c_{\text{out}} = 10$ km/s so that the central wavelength is 3.3 Mm. We choose to investigate the case where the source, receiver, and the center of the sphere containing the sound-speed perturbation are collinear. The geometry is shown in Figure 3.4. Note that everything in the problem is cylindrically symmetric about the line connecting the source and the receiver, which substantially simplifies the computations. We consider only the geometry where the sound-speed perturbation is midway between the source and the receiver, which are 90 Mm apart.

We consider two types of sound-speed perturbations. The first, which we refer to as the "uniform" case, is a perturbation that is uniform inside a sphere. The second, which we refer to as "smooth" is a sound-speed perturbation that tapers smoothly to zero at the surface of the sphere. For the "uniform" sphere the interior sound speed is

$$c_{\text{in}} = c_{\text{out}}(1 + A), \quad |\boldsymbol{x}| < R \tag{3.40}$$

and elsewhere the sound speed is the background sound speed, c_{out}. For the "smooth"

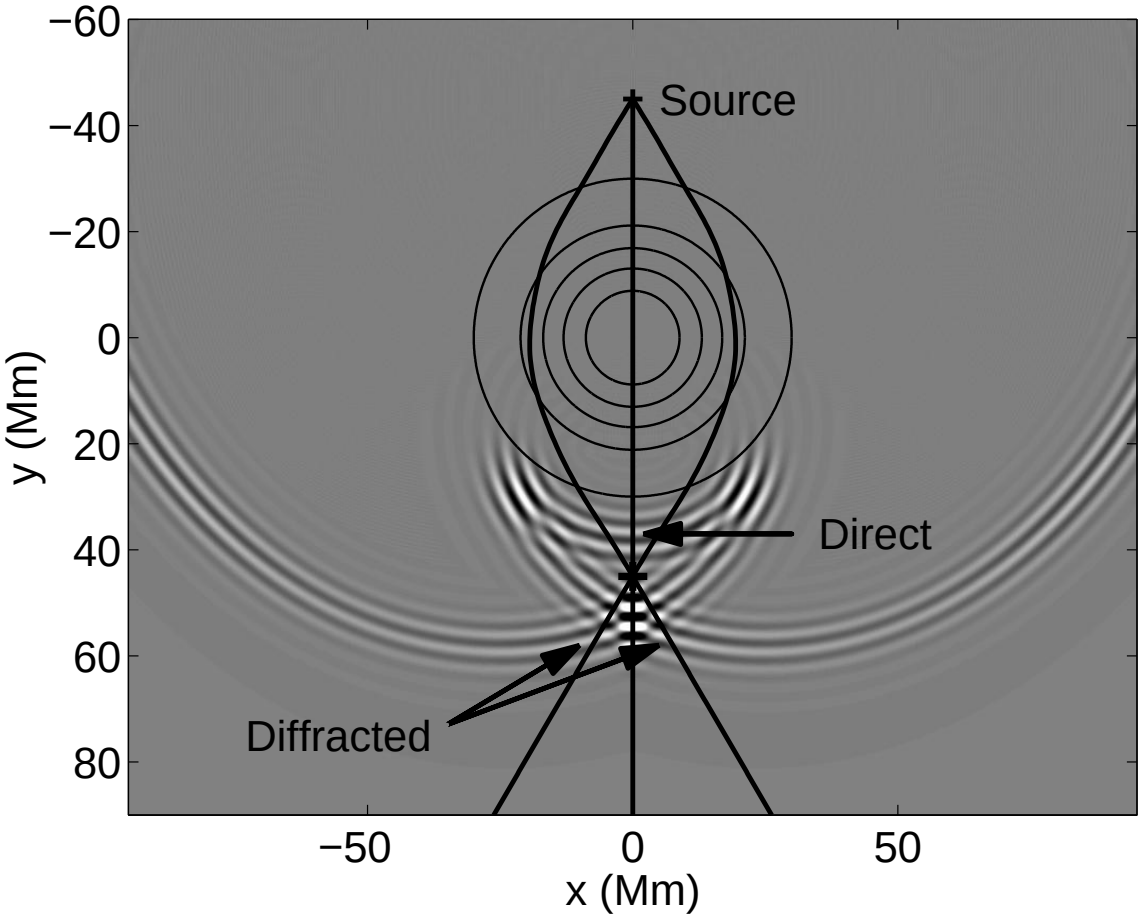

Figure 3.4: A frame from a finite difference calculation of the pressure field, shown as gray-scale, for the smooth sphere perturbation with $A = -0.5$ and $R = 15$ Mm. The source is at the upper black plus sign ($x = 0,\ y = -45$ Mm) and the receiver is at the lower ($x = 0,\ y = 45$ Mm). The black circles are contours of the sound speed, with the sound speed smallest in the innermost circle. The heavy black lines show the ray paths connecting, in the plane of the image, the source and the receiver. The two curved paths correspond to the diffracted wave, which avoids the slow center of the sphere. This is a cut through the three dimensional problem, but as the problem is cylindrically symmetric around the line $x = 0$ no information is lost.

sound-speed perturbation, the sound speed in the sphere is given by

$$c_{\text{in}}(\boldsymbol{x}) = c_{\text{out}} \left\{ 1 + \frac{A}{2} \left(1 + \cos \frac{\pi}{2} \frac{|\boldsymbol{x}|}{R} \right) \right\}, |\boldsymbol{x}| < 2R. \tag{3.41}$$

In both cases R is the HWHM of the perturbation and A is the maximum fractional sound-speed perturbation. Note that for both the uniform and smooth sound-speed perturbations the first-order ray theory travel-time perturbation is $-2AR/c_{\text{out}}$ for a ray going through the center of the sphere.

Although we calculate results for the pressure field directly, we are most interested in the travel-time perturbation associated with the sound-speed perturbation. As is becoming standard in geophysics (e.g. Hung et al., 2000) we define the travel-time perturbation as the time shift that maximizes the correlation between the unperturbed and perturbed waveforms. The cross-correlation we define as:

$$C(t) = \int \mathrm{d}t' \; p(\boldsymbol{x}_r, t') p_0(\boldsymbol{x}_r, t' - t) \tag{3.42}$$

where $p(\boldsymbol{x}_r, t')$ is the full waveform at the receiver and p_0 the waveform at the receiver in the absence of a sound-speed perturbation. The travel-time shift, Δt, is given by

$$C(\Delta t) = \text{maximum}. \tag{3.43}$$

3.3.1 Methods

We use four different methods to calculate travel times: first-order ray theory, the Born approximation, direct finite difference calculation of the wavefield, and for the case of the uniform sphere a spherical harmonic expansion. The ray theory we use is standard (e.g. Kosovichev & Duvall, 1997). The Born approximation we also apply in the usual way (e.g. Birch & Kosovichev, 2000). The spherical harmonic expansion, which we use for the uniform sphere case, is as in Morse & Feshbach (1953). For the direct finite difference calculation, which we apply to the smooth sphere case, we use an explicit 2-D code that takes advantage of the cylindrical symmetry of the problem (Schlottmann, 2000). To obtain travel times from the numerical waveforms we fit a parabola around the peak of the cross-correlation.

3.3.2 Results

We applied the techniques described in the previous section to a variety of cases, for both the uniform sphere and the smooth sound-speed perturbations described in Section 3.3. Figure 3.4 is a frame from a finite difference calculation of the pressure field, for a smooth sound-speed perturbation with $A = -0.5$ and $R = 15$ Mm. Waves are created at the source and move outwards, scattering from the sound-speed perturbation, and then are observed at the receiver. In this example the direct wave, which goes through the center of the sphere, arrives at the receiver after the diffracted wave, which goes around the center of the sphere. Notice that directly on axis the diffracted wave is focused and larger in amplitude than the direct wave. This is because for this geometry all of the diffracted waves add constructively at the receiver.

Figure 3.5 shows cross-correlations (Eq. [3.42]) for a variety of uniform and smooth spheres. We remind the reader that the travel-time perturbation associated with the sound-speed perturbation is the time lag that maximizes the cross correlation. Each panel summarizes the results for sphere HWHM between 0 and 25 Mm. For the weakest sound-speed perturbations, $A = \pm 0.01$, the cross-correlations for the uniform sphere, top pair of plots, mostly show the small shift in the peak of the cross-correlation to non-zero time lag, with the time shift accurately described by the Born approximation calculation (the black line). For spheres with $R > 15$ Mm the diffracted wave makes a visible contribution to the cross-correlation.

As the magnitude of the sound-speed perturbation is increased the diffracted wave becomes more important. For the $|A| = 0.05$ uniform sound-speed perturbations, shown in the middle pair of plots, the diffracted wave is in places stronger than the direct wave. The Born approximation travel time, however, remains associated with the direct wave part of the cross-correlation, most noticeably for $A = -0.05$ uniform spheres with $R > 20$ Mm. The third pair of plots is for the cases of the smooth spheres with $|A| = 0.05$. Here, unlike the uniform spheres with same value of A, an isolated diffracted wave is not visible.

We now look in detail at the numerical travel times and how they compare to the Born and ray approximation travel times. Results for the $A = \pm 0.01$ cases are summarized in the left panel of Figure 3.6. For these cases the Born approximation

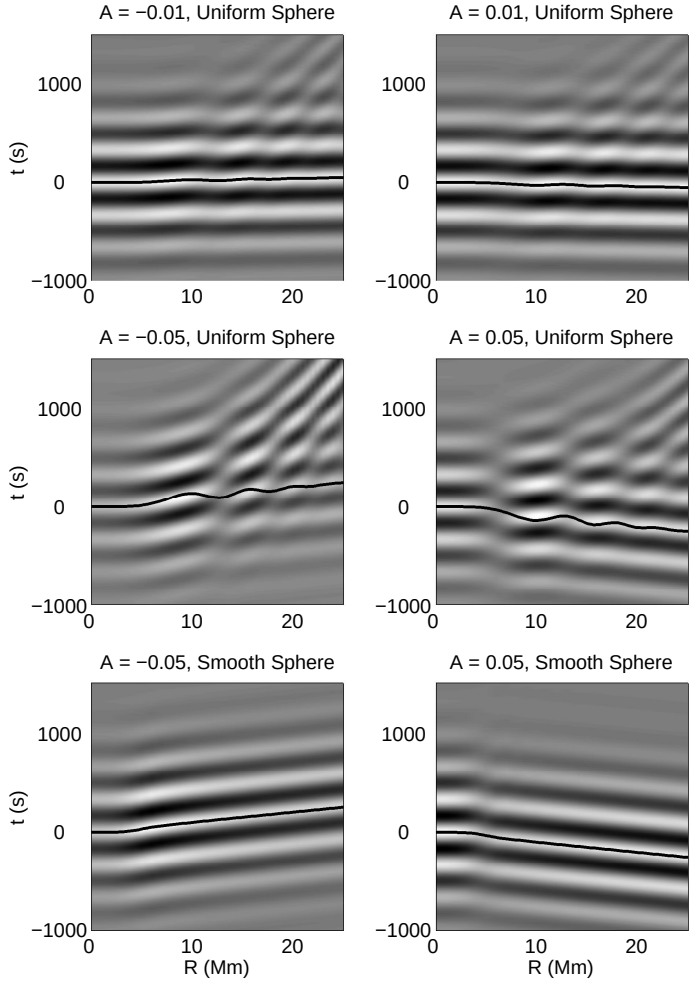

Figure 3.5: Cross-correlations between the waveform at the receiver and the unperturbed waveform for spheres of HWHM R with uniform and smooth sound-speed perturbations of various amplitudes. The gray-scale denotes the cross-correlation, with white corresponding to large positive values and black to large negative values. The black lines are the Born approximation travel times. For each plot the horizontal axis is sphere HWHM and the vertical axis is time lag. The top pair of panels is for uniform spheres with $|A| = 0.01$, the middle pair for uniform spheres with $|A| = 0.05$, and the bottom pair for smooth spheres with $|A| = 0.05$. The left column contains the negative sound-speed perturbations and the right column the positive.

travel time is always within two seconds of the numerical travel time. As sphere radius increases past the size of the first Fresnel zone, 8.2 Mm, the ray and Born approximations converge. At small radii the ray approximation overestimates travel times; this is a result of wave-front healing (Hung et al., 2001).

The right hand panel of Figure 3.6 shows travel times for the $A = \pm 0.05$ uniform sphere perturbations as functions of sphere radius. For the fast spheres the results are qualitatively the same as the $A = 0.01$ case although the Born approximation no longer captures the time delay fluctuations for intermediate sphere sizes. The $A = -0.05$ case is more complicated. For $R < 12$ Mm the diffracted wave and direct wave contributions cannot be separated; the numerical travel times for those spheres result from a mixture of the two types of waves. As is seen in Figure 3.5, for $R > 12$ Mm the cross-correlation exhibits two separate features, one corresponding to the direct wave and one to the diffracted wave. For the numerical travel time for $A = -0.05$, in Figure 3.6, we have plotted the location of the peak corresponding to the direct wave for $R > 12$ Mm. The rapid variation of the travel time near $R = 12$ Mm is a result of interference between the direct and diffracted waves.

In order to consider stronger perturbations, without the complications introduced by a strong diffracted wave, we also compute travel-time shifts for smooth spheres, see Figure 3.7. The travel times, in this case, do not oscillate with sphere radius, as they do in the uniform sphere case. This can be seen in the context of the Born approximation as the smooth sound-speed perturbation averaging the oscillations in the travel-time kernels. As in the uniform case the ray approximation substantially overestimates travel times for the small radii spheres. Also as in the uniform case the Born and first-order ray approximations converge in the large sphere limit. For large spheres the nonlinear dependence of the numerical travel time on A is visible. Unlike in the $|A| = 0.05$ cases, the effect of the diffracted wave is apparent for the $|A| = 0.1$ spheres, causing a visible difference between the Born approximation and the numerical travel times near $R = 5$ Mm.

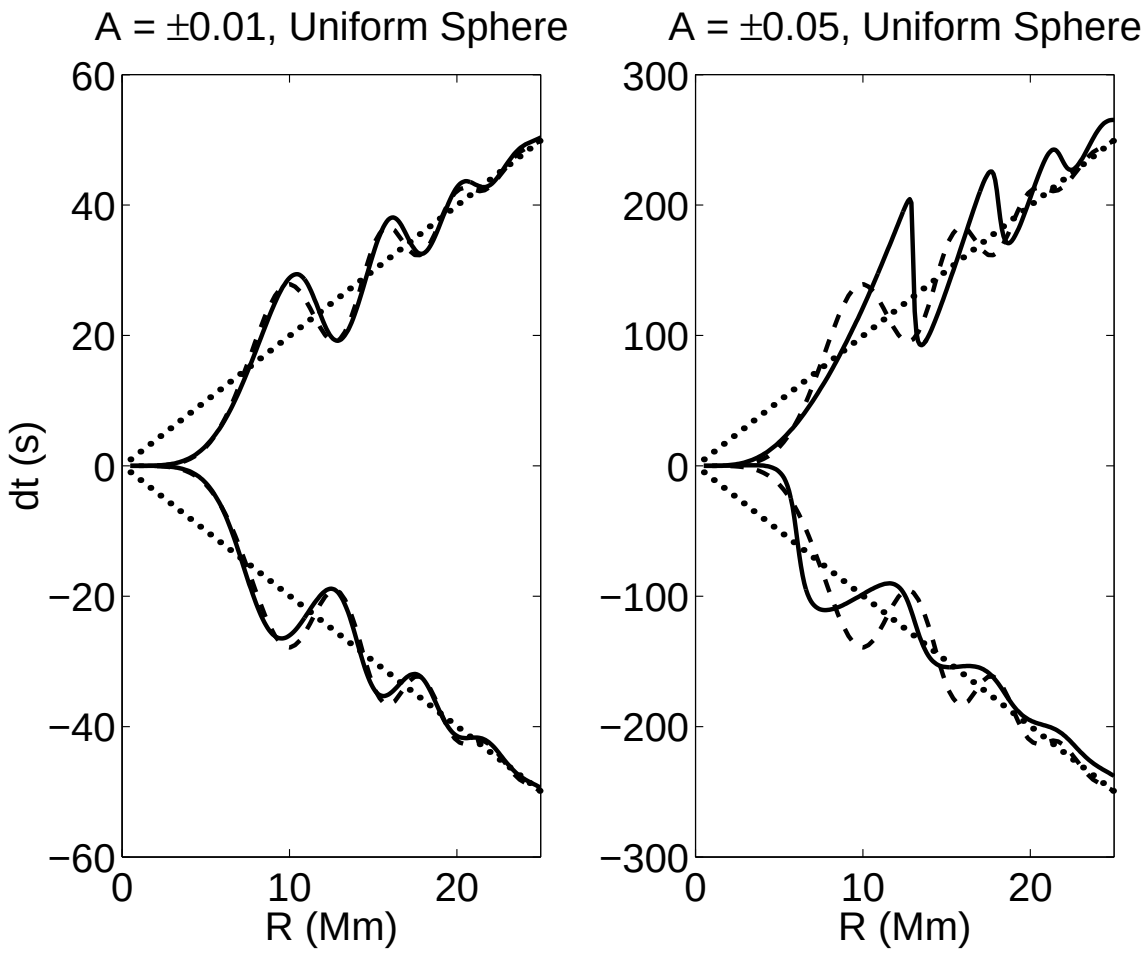

Figure 3.6: Travel-times shifts for uniform spheres as functions of sphere radius. The solid lines are the numerical results from the spherical harmonic expansion method. The dashed curves are the Born approximation. The dotted lines are the first order ray approximation. The left panel shows the two cases $A = \pm 0.01$. The right panel is for the cases $A = \pm 0.05$. For the case $A = -0.05$ the numerical time is shown for the peak in the cross-correlation that is closest to the Born approximation, although for $R > 12$ Mm the largest peak in the cross-correlation corresponds to the diffracted wave rather than the direct.

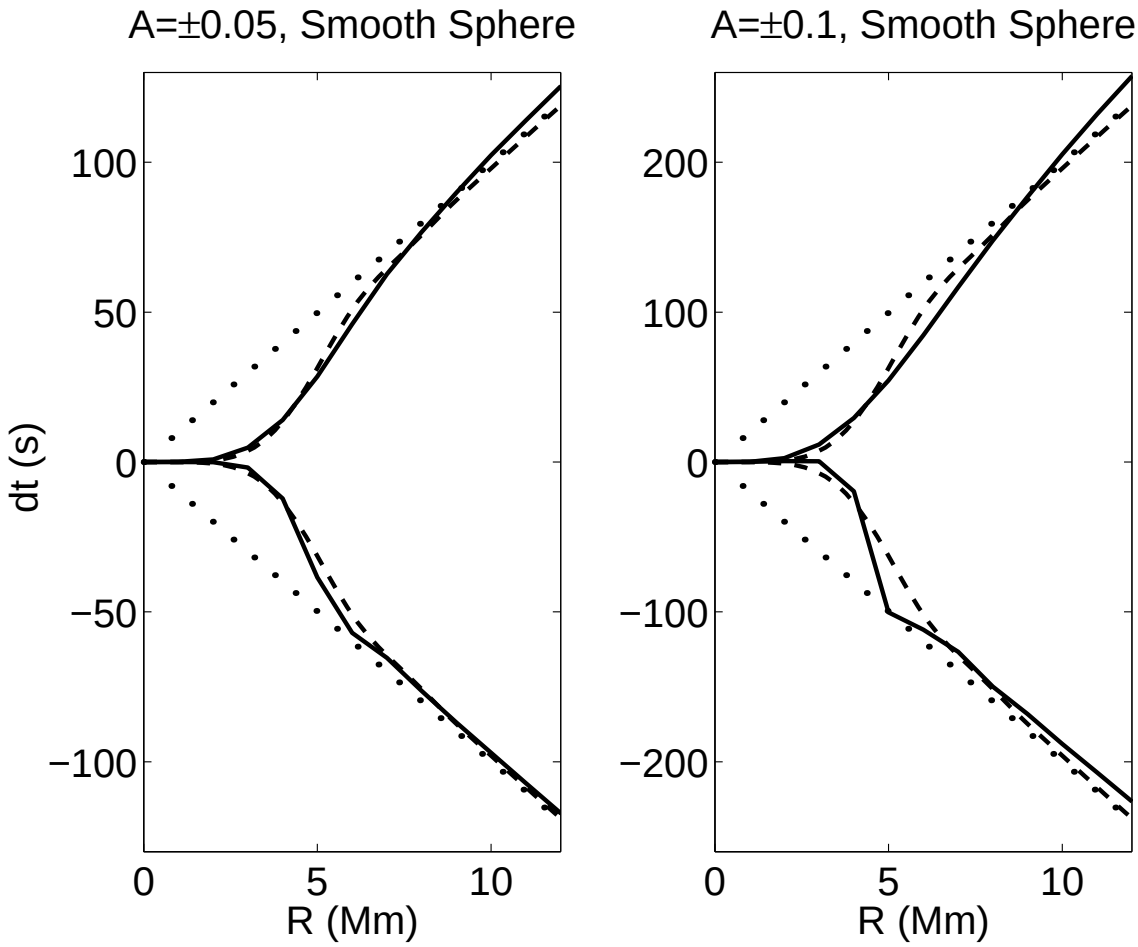

Figure 3.7: Travel times for smooth spheres as functions of sphere HWHM. The solid lines are the numerical results. The dashed curves are the Born approximation travel times and the dotted lines are the first-order ray approximation. The left panel shows the two cases $A = \pm 0.05$. The right panel is for the cases $A = \pm 0.1$.

3.4 A Distributed Source Model for Travel Time Sensitivities [1]

3.4.1 A General Theory

This section is an attempt to synthesize and extend the current knowledge into a flexible framework for the computation of the linear sensitivity of travel times to local inhomogeneities. We start from a physical description of the wave field, including wave excitation and damping. We incorporate the details of the measurement procedure. Two other key ingredients of our approach are the single-scattering Born approximation and a clear observational definition of travel time, both taken from the geophysics literature (e.g. Tong et al., 1998; Zhao & Jordan, 1998; Marquering et al., 1999). The main difference between the geophysics and helioseismology problems is that helioseismology deals with multiple random wave sources as opposed to a single isolated source.

The next section, 3.4.2, is an example calculation of travel time kernels for surface gravity waves. The purpose is to demonstrate the application of the general theory described in this section. We compute travel-time kernels for local perturbations in source strength and damping rate. In our model, these perturbations are confined to the surface and therefore are computationally convenient as we obtain two-dimensional kernels. Localized source and damping perturbations are interesting and not yet well understood. For this example, we also compare these kernels with kernels calculated in the single-source picture (Birch & Kosovichev, 2000; Jensen et al., 2000), in which the effect of distributed random sources is approximated by a single causal source at the observation point $\mathbf{1}$. We show that the single-source kernels do not reproduce all the features seen in the distributed-source kernels.

We define the "travel time" for each branch to be the time lag that minimizes the difference between the measured cross-correlation, C, and a sliding reference wavelet, C^{ref}. Depending on the choice of reference wavelet the term "travel time" may be an abuse of language; this issue will be clarified later. The travel time for

[1] *This section is essentially the ApJ paper with L. Gizon (Gizon & Birch, 2002). That paper was a work of equal collaboration.*

waves going from **1** to **2** is denoted by $\tau_+(\mathbf{1},\mathbf{2})$ and the travel time for waves going from **2** to **1** by $\tau_-(\mathbf{1},\mathbf{2})$. The difference (in the least squares sense) between the observed cross-correlation and the reference wavelet is

$$X_\pm(\mathbf{1},\mathbf{2},t) = \int_{-\infty}^{\infty} \mathrm{d}t'\, f(\pm t')\left[C(\mathbf{1},\mathbf{2},t') - C^{\mathrm{ref}}(\mathbf{1},\mathbf{2},t' \mp t)\right]^2 . \tag{3.44}$$

The window function, $f(t')$, is a one-sided function (zero for t' negative) used to separately examine the positive- and negative-time parts of the cross-correlation. The window $f(t')$ is used to measure τ_+, and $f(-t')$ is used to measure τ_-. One possible choice is a window that isolates the first-skip branch of the cross-correlation. Other window functions could be chosen to, for example, isolate the second bounce branch of a cross-correlation in the case of acoustic modes.

By definition the travel times $\tau_\pm$ are the time lags that minimize $X_\pm$:

$$\tau_\pm(\mathbf{1},\mathbf{2}) = \underset{t}{\mathrm{argmin}}\{\, X_\pm(\mathbf{1},\mathbf{2},t)\,\}\,. \tag{3.45}$$

Minimizing $X_\pm$ is equivalent to fitting $C^{\mathrm{ref}}(t' \mp t)$ to $C(t')$ with a weighting in time given by $f(\pm t')$, varying the time lag t only. An example of measuring the travel times $\tau_\pm$ from a cross-correlation is shown in Figure 3.8.

The choice of reference wavelet $C^{\mathrm{ref}}(\mathbf{1},\mathbf{2},t)$ is left to the observer. For most applications the reference wavelet needs only be a function of distance $\Delta = \|\mathbf{2}-\mathbf{1}\|$ and time t. As was done in Figure 3.8, one possible choice is to take C^{ref} to look like a cross-correlation. In this case τ_+ and τ_- are small and the term "travel time" should be understood to mean "time lag". A reference wavelet that resembles a cross-correlation can be constructed by either averaging the observed cross-correlations over all possible pairs of points $(\mathbf{1},\mathbf{2})$ for each distance Δ (see Fig. 1.1), or by computing a theoretical cross-correlation from a solar model (see § 3.4.2). Another possible choice is to take $C^{\mathrm{ref}}(\mathbf{1},\mathbf{2},t)$ to look like a single wavelet centered about $t = 0$. In this case τ_+ and τ_- will essentially represent the time it takes for wavepackets to travel between the observation points, and the denomination "travel times" for $\tau_\pm$ is appropriate.

The definition of travel time presented here is analogous to the typical definition of travel time used in the geophysics literature (e.g. Zhao & Jordan, 1998). In

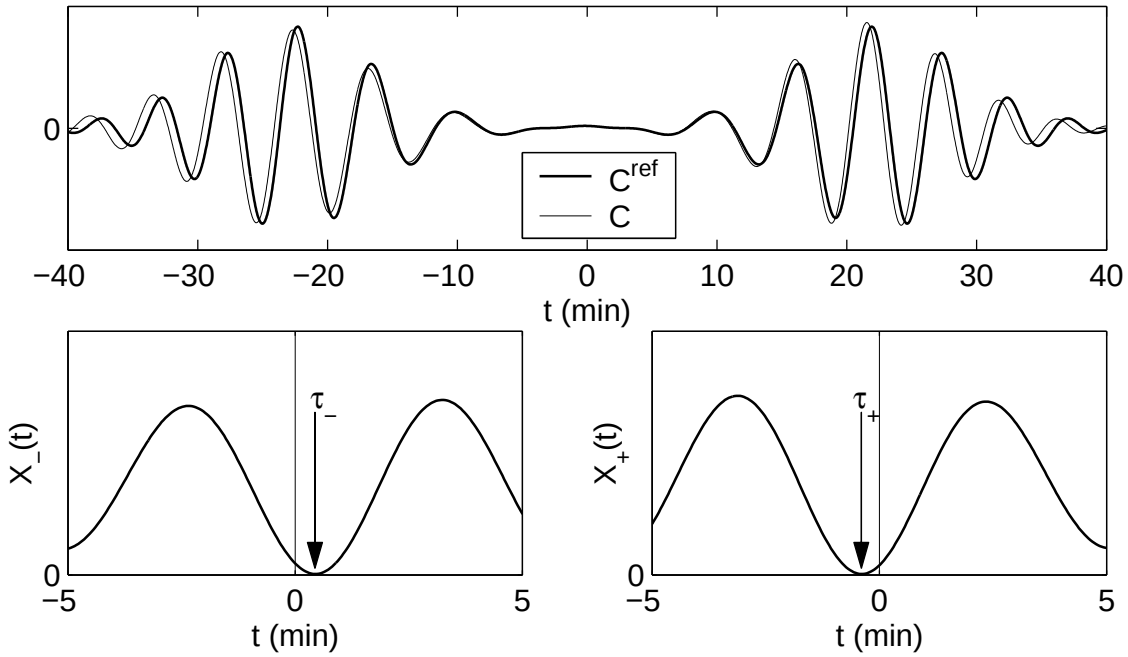

Figure 3.8: An example showing how to measure the travel times $\tau_\pm$ from a cross-correlation $C(\mathbf{1}, \mathbf{2}, t)$. In this figure we choose the reference wavelet $C^{\rm ref}$ (heavy line in top panel) to be the zero-order cross-correlation, for the distance $\Delta = 10$ Mm, from the surface gravity wave example discussed in Section 3.4.2. In general, the observer is free to choose any reference wavelet. This function, $C^{\rm ref}$, is even in time. The light line (top panel) shows an example cross-correlation, C, which in this particular case was computed from a model including a uniform horizontal flow of 400 m s^{-1} in the direction $\mathbf{1} \rightarrow \mathbf{2}$. To measure the travel times $\tau_\pm$ from C we need to minimize the functions $X_\pm$. The lower panels show the functions $X_-(t)$ and $X_+(t)$, constructed using equation (3.44). The window function f was chosen to be the Heaviside step function. For the positive-time branch of C, the best fit is obtained by shifting $C^{\rm ref}$ toward $t = 0$ (to the left). The minimum of $X_+(t)$ occurs at a negative time τ_+, as can be seen in the right bottom panel. For the negative-time branch of C, the minimum of the function $X_-(t)$ occurs at a positive time τ_- (see bottom left panel). The locations, τ_- and τ_+, of the minima of the functions $X_-(t)$ and $X_+(t)$ are, by definition, the measured travel times. In this particular example the signs $\tau_+ < 0$ and $\tau_- > 0$ make sense as waves travel faster with the flow than against it.

time-distance helioseismology Duvall et al. (1997) measure travel times by fitting a Gaussian wavelet to cross-correlations. This procedure distinguishes between group and phase travel times, by allowing both the envelope and phase of the wavelet to vary independently. Our definition is a simplification of this procedure as it contains only one travel-time parameter per branch. The travel time defined here is neither a pure group nor phase time; it is, however, perfectly well defined and has already been used in a time-distance study with real data (Gizon et al., 2000). Without significant difficulty, the fitting presented here could be extended to include more parameters, for example amplitude and central frequency, as is done by Duvall et al. (1997).

Traditionally, mean and difference travel times have been used in place of the one-way travel times. The mean and difference travel times are obtained from the one-way travel times by

$$\tau_{\rm mean} = \frac{1}{2}(\tau_+ + \tau_-)\,, \tag{3.46}$$

$$\tau_{\rm diff} = \tau_+ - \tau_-\,. \tag{3.47}$$

The motivation behind using $\tau_{\rm mean}$ and $\tau_{\rm diff}$ is that sound-speed perturbations are expected to contribute mostly to the mean travel time and flows to the travel-time difference (e.g. Kosovichev & Duvall, 1997).

The definition of travel-time perturbations described here leaves observers free to measure without reference to a solar model. We note, however, that in order for a proper interpretation of measured travel-time perturbations to be made it is essential for observers to report their choices of reference wavelet $C^{\rm ref}$, window function f, and filter $\mathcal{F}$. A solar model is only necessary for the next step, the interpretation of travel-time perturbations in terms of local perturbations to a solar model, to which we now turn.

Interpretation of Travel Times

The goal of time-distance helioseismology is to estimate the internal solar properties which produce model travel times that best match observed travel times. To achieve this, we need to know how to compute the travel times for a particular solar model.

In order to make the inverse problem feasible we also need to linearize the forward problem around a background state that is close to the Sun.

A background solar model is fully specified by a set of internal properties (density, pressure, etc.) which we denote by $q_\alpha(\boldsymbol{r})$ for short. Standard solar models provide a reasonable background state. In the background state the cross-correlation and the travel times are C^0 and $\tau_\pm^0$ respectively. We then consider small perturbations, $\delta q_\alpha(\boldsymbol{r})$, to the solar properties. These perturbations could include, for example, local changes in density, sound speed, or flows. The difference between the resulting cross-correlation, C, and the background cross-correlation we denote by δC,

$$\delta C(\mathbf{1},\mathbf{2},t) = C(\mathbf{1},\mathbf{2},t) - C^0(\mathbf{1},\mathbf{2},t)\,. \tag{3.48}$$

Likewise, the perturbed travel times $\delta\tau_\pm$ are

$$\delta\tau_\pm(\mathbf{1},\mathbf{2}) = \tau_\pm(\mathbf{1},\mathbf{2}) - \tau_\pm^0(\mathbf{1},\mathbf{2})\,. \tag{3.49}$$

The travel times $\tau_\pm(\mathbf{1},2)$ are measured from the cross-correlation $C(\mathbf{1},\mathbf{2},t)$. The reference times $\tau_\pm^0$ are the travel times which would be measured if the Sun and the background model were identical.

As we are considering small changes in the solar model, the correction to the model cross-correlation, δC, will also be small. As a result we can linearize the dependence of the travel-time perturbations $\delta\tau_\pm$ on δC. The algebra is detailed in Appendix B. The result of this calculation can be written as

$$\delta\tau_\pm(\mathbf{1},\mathbf{2}) = \int_{-\infty}^{\infty} \mathrm{d}t\; W_\pm(\mathbf{1},\mathbf{2},t)\,\delta C(\mathbf{1},\mathbf{2},t)\,. \tag{3.50}$$

The functions $W_\pm$ depend on the zero-order cross-correlation C^0, the reference wavelet C^{ref}, and the window function f, and are given in equation (B.7). The sensitivity of $\delta\tau_\pm$ to δC is given by the weight functions $W_\pm$. We emphasize that the travel-time perturbations $\delta\tau_\pm$ are proportional to δC, which is a first-order perturbation to the background solar model. We interpret the right-hand side of equation (3.50) as a model for the difference between the observed travel times and the theoretical travel times in the background solar model.

The source of solar oscillations is turbulent convection near the solar surface (e.g. Stein, 1967). As a result the signal ϕ and the cross-correlation C are realizations of a random process. In general, a random variable is fully characterized by its expectation value and all of its higher-order moments. As a result, to describe a travel-time perturbation $\delta\tau$ we need its expectation value (ensemble average) as well as its variance, etc. In this paper we consider only the expectation value. A calculation of the variance of the travel times would be essential to characterize the realization noise in travel-time measurements. An accurate estimate of the noise in travel-time measurements is important for solving the inverse problem.

In this paper we only compute the expectation values of travel-time perturbations and cross-correlations. This represents a first and necessary step. Notice in addition that under the assumptions of the Ergodic theorem (e.g. Yaglom, 1962) the cross-correlations (hence travel times) tend to their expectation values as the observational time interval increases.

Modeling the Observed Signal

In order to obtain the cross-correlation, C^0, and its first-order perturbation, δC, we need to compute the observable, ϕ, defined in equation (1.19), and therefore the wave velocity $\boldsymbol{v}$. Linear oscillations are governed by an equation of the form (e.g. Gough, 1987)

$$\boldsymbol{\mathcal{L}v} = \boldsymbol{S}\,. \tag{3.51}$$

The vector $\boldsymbol{S}$ denotes the source of excitation for the waves. The linear operator $\boldsymbol{\mathcal{L}}$, acting on $\boldsymbol{v}$, should encompass all the physics of wave propagation in an inhomogeneous stratified medium permeated by flows and magnetic fields. Damping processes should also be accounted for in $\boldsymbol{\mathcal{L}}$. An explicit expression for the operator $\boldsymbol{\mathcal{L}}$ including steady flows is provided by Lynden-Bell & Ostriker (1967). Bogdan (2000) includes magnetic field.

We now expand $\boldsymbol{\mathcal{L}}$, $\boldsymbol{v}$, and $\boldsymbol{S}$ into zero- and first-order contributions, which refer

to the background solar model and to the lowest-order perturbation to that model:

$$\mathcal{L} = \mathcal{L}^0 + \delta\mathcal{L}\,, \tag{3.52}$$

$$\boldsymbol{v} = \boldsymbol{v}^0 + \delta\boldsymbol{v}\,, \tag{3.53}$$

$$\boldsymbol{S} = \boldsymbol{S}^0 + \delta\boldsymbol{S}\,. \tag{3.54}$$

The operator $\delta\mathcal{L}$ depends on first-order quantities such as local perturbations in density, sound speed, and damping rate, as well as flows and magnetic field. In general, one may contemplate time-dependent perturbations. There are, however, many interesting structures on the Sun (e.g. supergranules, meridional flow, moat flows) which are approximately time independent on the time scale on which time-distance measurements are made (at least several hours). As a result, for the sake of simplicity, we only consider time-independent perturbations. These perturbations, which we denote by $\delta q_\alpha(\boldsymbol{r})$ for short, are thus only functions of position $\boldsymbol{r}$ in the solar interior.

To lowest order, equation (3.51) reduces to

$$\mathcal{L}^0\boldsymbol{v}^0 = \boldsymbol{S}^0\,. \tag{3.55}$$

In order to solve this equation, we introduce a set of causal Green's vectors $\boldsymbol{G}^i$ defined by

$$\mathcal{L}^0\boldsymbol{G}^i(\boldsymbol{x},t;\boldsymbol{s},t_\mathrm{s}) = \hat{\boldsymbol{e}}_i(\boldsymbol{s})\,\delta_\mathrm{D}(\boldsymbol{x}-\boldsymbol{s})\,\delta_\mathrm{D}(t-t_\mathrm{s})\,, \tag{3.56}$$

where the $\hat{\boldsymbol{e}}_i(\boldsymbol{s})$ are three orthogonal basis vectors at the point $\boldsymbol{s}$ and δ_D is the Dirac delta function. The vector $\boldsymbol{G}^i(\boldsymbol{x},t;\boldsymbol{s},t_\mathrm{s})$ is the velocity at location $\boldsymbol{x}$ and time t which results from a unit impulsive source in the $\hat{\boldsymbol{e}}_i$ direction at time t_s and location $\boldsymbol{s}$. Note that the vector $\boldsymbol{G}^i$ does not in general point in the direction of $\hat{\boldsymbol{e}}_i$. Guided by equation (1.19), we define the zero-order Green's functions for the observable ϕ:

$$\mathcal{G}^i(\boldsymbol{x},t;\boldsymbol{s},t_\mathrm{s}) = \mathcal{F}\left\{\hat{\boldsymbol{\ell}}(\boldsymbol{x})\cdot\boldsymbol{G}^i(\boldsymbol{x},t;\boldsymbol{s},t_\mathrm{s})\right\}\,. \tag{3.57}$$

In terms of $\mathcal{G}^i$, the unperturbed signal reads:

$$\phi^0(\boldsymbol{x},t) = \int_\odot \mathrm{d}\boldsymbol{s}\int_{-\infty}^{\infty}\mathrm{d}t_\mathrm{s}\;\mathcal{G}^i(\boldsymbol{x},t;\boldsymbol{s},t_\mathrm{s})\,S_i^0(\boldsymbol{s},t_\mathrm{s})\,. \tag{3.58}$$

The sum is taken over the repeated index i, as is done for all repeated indexes throughout this paper.

To the next order of approximation, equation (3.51) gives

$$\mathcal{L}^0\,\delta\boldsymbol{v} = -\delta\mathcal{L}\,\boldsymbol{v}^0 + \delta\boldsymbol{S}\,. \tag{3.59}$$

This is the single-scattering Born approximation (e.g. Sakurai, 1995). The first-order Born approximation has been shown to work for small perturbations (e.g. Hung et al., 2000; Birch et al., 2001a). We note that equation (3.59) is of the same form as equation (3.55): the term $-\delta\mathcal{L}\,\boldsymbol{v}^0+\delta\boldsymbol{S}$ appears as a source for the scattered wave velocity $\delta\boldsymbol{v}$. The solution to equation (3.59) is thus

$$\delta\boldsymbol{v}(\boldsymbol{x},t) = \int_\odot \mathrm{d}\boldsymbol{s} \int_{-\infty}^{\infty} \mathrm{d}t_s\; \boldsymbol{G}^i(\boldsymbol{x},t;\boldsymbol{s},t_s)\big\{-\delta\mathcal{L}\boldsymbol{v}^0(\boldsymbol{s},t_s) + \delta\mathbf{S}(\boldsymbol{s},t_s)\big\}_i\,, \tag{3.60}$$

where $\{\cdot\}_i$ denotes the i-th component of the vector inside the curly braces.

By expressing the zero-order velocity $\boldsymbol{v}^0$ in terms of the Green's function and the source, and using equations (3.60) and $\delta\phi = \mathcal{F}\{\hat{\boldsymbol{\ell}}\cdot\delta\boldsymbol{v}\}$, the perturbed signal can be written as

$$\begin{aligned}\delta\phi(\boldsymbol{x},t) \;=\; & \int_\odot \mathrm{d}\boldsymbol{r} \int_{-\infty}^{\infty} \mathrm{d}t' \int_\odot \mathrm{d}\boldsymbol{s} \int_{-\infty}^{\infty} \mathrm{d}t_\mathrm{s}\; \mathcal{G}^i(\boldsymbol{x},t;\boldsymbol{r},t')\big\{-\delta\mathcal{L}\boldsymbol{G}^j(\boldsymbol{r},t';\boldsymbol{s},t_\mathrm{s})\big\}_i\, S_j^0(\boldsymbol{s},t_\mathrm{s}) \\ & + \int_\odot \mathrm{d}\boldsymbol{s} \int_{-\infty}^{\infty} \mathrm{d}t_\mathrm{s}\; \mathcal{G}^i(\boldsymbol{x},t;\boldsymbol{s},t_\mathrm{s})\,\delta S_i(\boldsymbol{s},t_\mathrm{s})\,. \end{aligned} \tag{3.61}$$

We recall that the operator $\delta\mathcal{L}$ contains the first-order perturbations to the solar model, $\delta q_\alpha(\boldsymbol{r})$. The first term in the above equation contains two Green's functions; it represents the contribution to $\delta\phi(\boldsymbol{x},t)$ that comes from a wave that is created by the source at location $\boldsymbol{s}$ at time t_s, is scattered at time t' by the perturbations at location $\boldsymbol{r}$, and then propagates to the location $\boldsymbol{x}$. The details of the scattering process are encoded in the operator $\delta\mathcal{L}$. The second term results from the perturbation to the source function, and involves only a single Green's function, which propagates waves from the location and time of the source to the observation location and time. As we now have ϕ^0 and $\delta\phi$ we can next compute the zero- and first-order cross-correlations, C^0 and δC.

Temporal Cross-Correlation

We remind the reader that we only want to compute the expectation value of the cross-correlation. In the rest of this paper, cross-correlations stand for their expectation values. From equation (1.20) and equation (3.58) for ϕ^0 we deduce a general expression for the zero-order cross-correlation:

$$\begin{aligned} C^0(\mathbf{1},\mathbf{2},t) &= \frac{1}{T}\int \mathrm{d}t'\,\mathrm{d}\boldsymbol{s}\,\mathrm{d}t_\mathrm{s}\,\mathrm{d}\boldsymbol{s}'\,\mathrm{d}t'_\mathrm{s}\; M^0_{ij}(\boldsymbol{s},t_\mathrm{s};\boldsymbol{s}',t'_\mathrm{s}) \\ &\quad \times \mathcal{G}^i(\mathbf{1},t';\boldsymbol{s},t_\mathrm{s})\,\mathcal{G}^j(\mathbf{2},t'+t;\boldsymbol{s}',t'_\mathrm{s})\,, \end{aligned} \tag{3.62}$$

with

$$M^0_{ij}(\boldsymbol{s},t_\mathrm{s};\boldsymbol{s}',t'_\mathrm{s}) = \mathrm{E}\left[S^0_i(\boldsymbol{s},t_\mathrm{s})\,S^0_j(\boldsymbol{s}',t'_\mathrm{s})\right], \tag{3.63}$$

where $\mathrm{E}[\cdot]$ denotes the expectation value of the expression in square brackets. For the sake of readability, we have omitted the limits of integration in equation (3.63). The matrix $\mathbf{M}^0$ gives the correlation between any two components of $\boldsymbol{S}^0$, measured at two possibly different positions.

No assumption has been made about $\mathbf{M}^0$ to obtain equation (3.62). With the assumptions of stationarity in time and homogeneity and isotropy in the horizontal direction, $\mathbf{M}^0$ only depends on the time difference $t_\mathrm{s}-t'_\mathrm{s}$, the horizontal distance between $\boldsymbol{s}$ and $\boldsymbol{s}'$, and their depths. Further assumptions could be made in order to simplify the computation of equation (3.62). In the spirit of Woodard (1997) one might assume that the sources are spatially uncorrelated or are located only at a particular depth. A better approach might be to obtain the statistical properties of $\boldsymbol{S}^0$ from recent numerical simulations of solar convection (e.g. Stein & Nordlund, 2000) or observations of photospheric convection (e.g. Title et al., 1989; Chou et al., 1991; Strous et al., 2000). Furthermore, a comparison of models and observations of the power spectrum of solar oscillations can be used to constrain the depths and types of sources (e.g. Duvall et al., 1993a).

We now perturb equation (1.20) and take the expectation value to obtain

$$\delta C(\mathbf{1},\mathbf{2},t) = \frac{1}{T}\int_{-\infty}^{\infty}\mathrm{d}t'\,\mathrm{E}\left[\delta\phi(\mathbf{1},t')\,\phi^0(\mathbf{2},t'+t)+\phi^0(\mathbf{1},t')\,\delta\phi(\mathbf{2},t'+t)\right]. \tag{3.64}$$

The function δC has two contributions, one from the perturbation to the wave

operator, $\delta C_{\mathcal{L}}$, and one from the source perturbation, δC_S :

$$\delta C = \delta C_{\mathcal{L}} + \delta C_S \,. \tag{3.65}$$

Using the expressions for ϕ^0 and $\delta\phi$ given by equations (3.58) and (3.61), we obtain the perturbation to the cross-correlation resulting from a change in the wave operator $\boldsymbol{\mathcal{L}}$:

$$\begin{aligned}
\delta C_{\mathcal{L}}(\mathbf{1},\mathbf{2},t) \;=\; & \frac{1}{T}\int_{\odot} \mathrm{d}\boldsymbol{r} \int \mathrm{d}t'\,\mathrm{d}t''\,\mathrm{d}\boldsymbol{s}\,\mathrm{d}t_{\mathrm{s}}\,\mathrm{d}\boldsymbol{s}'\,\mathrm{d}t'_{\mathrm{s}} \\
& \times \left\{-\delta\boldsymbol{\mathcal{L}}\boldsymbol{G}^i(\boldsymbol{r},t'';\boldsymbol{s},t_{\mathrm{s}})\right\}_k M^0_{ij}(\boldsymbol{s},t_{\mathrm{s}};\boldsymbol{s}',t'_{\mathrm{s}}) \\
& \times \left[\mathcal{G}^j(\mathbf{2},t'+t;\boldsymbol{s}',t'_{\mathrm{s}})\,\mathcal{G}^k(\mathbf{1},t';\boldsymbol{r},t'')\right. \\
& \left. + \mathcal{G}^j(\mathbf{1},t';\boldsymbol{s}',t'_{\mathrm{s}})\,\mathcal{G}^k(\mathbf{2},t'+t;\boldsymbol{r},t'')\right] .
\end{aligned} \tag{3.66}$$

The above equation, which gives the perturbation to the cross-correlation due to scattering, has two components, illustrated in Figure 3.9a. The first component comes from the correlation of the scattered wave at $\mathbf{1}$ with the direct wave at $\mathbf{2}$, i.e. $\delta\phi(\mathbf{1},t')\phi^0(\mathbf{2},t'+t)$, and the second component comes from $\phi^0(\mathbf{1},t')\delta\phi(\mathbf{2},t'+t)$. Both these components appear in equation (3.66) as the product of three Green's functions. From the term $\delta\phi(\mathbf{1},t')\phi^0(\mathbf{2},t'+t)$ there is one Green's function for the wave that goes directly from $\boldsymbol{s}'$ to $\mathbf{2}$, which gives $\phi^0(\mathbf{2})$. There is a second Green's function for the wave that is created at $\boldsymbol{s}$ and travels to $\boldsymbol{r}$, and the third Green's function takes the scattered wave from $\boldsymbol{r}$ to $\mathbf{1}$, which gives $\delta\phi(\mathbf{1})$. The term $\phi^0(\mathbf{1},t')\delta\phi(\mathbf{2},t'+t)$ can be understood by switching the roles of $\mathbf{1}$ and $\mathbf{2}$. The scattering process is described by the operator $\delta\boldsymbol{\mathcal{L}}$, which depends on the perturbations $\delta q_\alpha(\boldsymbol{r})$. The Green's function $\mathcal{G}$ is used for waves that arrive at an observation point as it gives the response of ϕ to a source. The Green's vectors $\boldsymbol{G}^i$ are used to propagate the wave velocity from a source to the scattering point, as the scattered wave depends on the vector velocity of the incoming wave.

The cross-correlation is also sensitive to changes in the source function. The first-order perturbation resulting from a small change in the source function can be

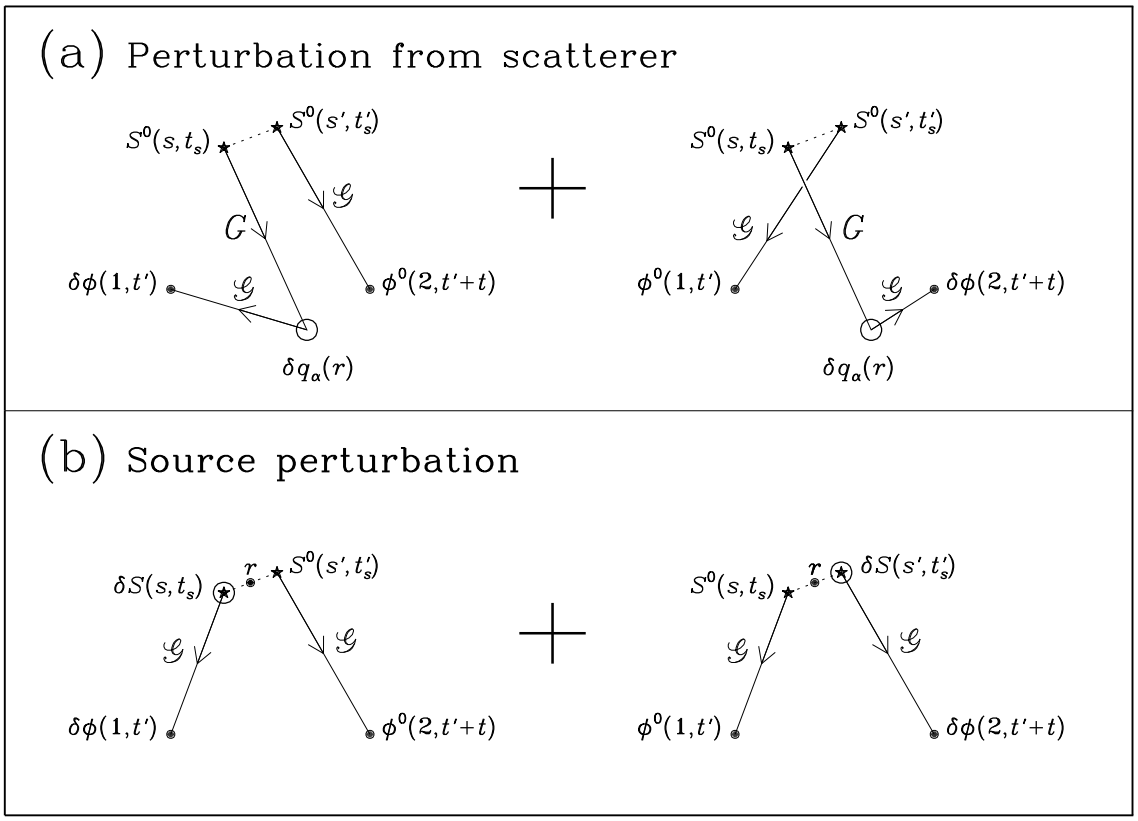

Figure 3.9: A graphical representation of the two types of contributions to the first-order perturbation to the cross-correlation (eqs [3.66] and [3.67]). Panel (a) is for scattering from perturbations $\delta q_\alpha(\boldsymbol{r})$ to the model and panel (b) is for changes $\delta \boldsymbol{S}$ in the source function. Scattering processes contribute to the cross-correlation as the product of three Green's functions: one Green's function to describe the direct wave from the source to an observation point and two Green's functions to obtain the scattered wave at the other observation point, in the Born approximation. The sensitivity of the cross-correlation to a change in the source function only involves two Green's functions, one to propagate waves from the unperturbed source to an observation point and one to give the response, at the other observation point, to the change in the source function. Throughout the diagram, as in the text, the Green's function for the observable is given by $\mathcal{G}$ and the Green's function for the vector velocity is $\boldsymbol{G}$. The dotted line between the source locations, $\boldsymbol{s}$ and $\boldsymbol{s'}$, indicates that the two sources are connected through the source covariance matrix $\mathbf{M}$.

written as (from eqs. [3.58] and [3.61])

$$\begin{aligned}\delta C_S(\mathbf{1},\mathbf{2},t) &= \frac{1}{T}\int \mathrm{d}t'\,\mathrm{d}\boldsymbol{s}\,\mathrm{d}t_\mathrm{s}\,\mathrm{d}\boldsymbol{s}'\,\mathrm{d}t'_\mathrm{s}\;\delta M_{ij}(\boldsymbol{s},t_\mathrm{s};\boldsymbol{s}',t'_\mathrm{s}) \\ &\quad\times \mathcal{G}^i(\mathbf{1},t';\boldsymbol{s},t_\mathrm{s})\,\mathcal{G}^j(\mathbf{2},t'+t;\boldsymbol{s}',t'_\mathrm{s})\,, \end{aligned} \tag{3.67}$$

where the perturbation to the source covariance is:

$$\delta M_{ij}(\boldsymbol{s},t_\mathrm{s};\boldsymbol{s}',t'_\mathrm{s}) = \mathrm{E}\left[S^0_i(\boldsymbol{s},t_\mathrm{s})\;\delta S_j(\boldsymbol{s}',t'_\mathrm{s}) + \delta S_i(\boldsymbol{s},t_\mathrm{s})\;S^0_j(\boldsymbol{s}',t'_\mathrm{s})\right]\,. \tag{3.68}$$

Figure 3.9b gives a graphical interpretation of equation (3.67). Unlike the perturbation to the cross-correlation due to scattering, equation (3.67) contains only two Green's functions. One connects the unperturbed source with the unperturbed signal at an observation point, while the second relates the source perturbation to the perturbed signal at the other observation point.

Later in this paper it will be necessary to express the perturbation to the cross-correlation as a spatial integral over the location, $\boldsymbol{r}$, of the perturbation to the solar model. In order to be able to write equation (3.67) for δC_S in this form, we introduce the change of variable $\boldsymbol{r} = (\boldsymbol{s}+\boldsymbol{s}')/2$ and $\boldsymbol{u} = \boldsymbol{s}-\boldsymbol{s}'$. This change of variable is also useful because we expect the source covariance $\mathbf{M}$ to be small for large $\boldsymbol{u}$, i.e. for sources that are far apart. In the limit of very small source correlation length, $\mathbf{M}$ is a function only of $\boldsymbol{r}$.

We have shown how to obtain C^0 and δC from an assumed solar model consisting of a background model ($\boldsymbol{\mathcal{L}}^0$ and $\boldsymbol{S}^0$) and small perturbations ($\delta\boldsymbol{\mathcal{L}}$ and $\delta\boldsymbol{S}$). Earlier we showed how to connect perturbations to the cross-correlation to travel-time perturbations. Next we put these pieces together and obtain travel-time kernels, which give the travel-time perturbations resulting from small changes in the solar model.

Travel-Time Sensitivity Kernels

It is useful for the derivation of travel-time kernels to express the perturbation to the cross-correlation δC as an integral over the location $\boldsymbol{r}$ of the perturbations $\delta q_\alpha(\boldsymbol{r})$. In general $\delta\boldsymbol{\mathcal{L}}$ and $\delta\mathbf{M}$ involve spatial derivatives of the perturbations $\delta q_\alpha(\boldsymbol{r})$ to the solar model and so integration by parts on the variable $\boldsymbol{r}$ may be required to obtain,

from equations (3.65), (3.66), and (3.67) a relationship of the form:

$$\delta C(\mathbf{1},\mathbf{2},t) = \int_{\odot} \mathrm{d}\boldsymbol{r}\; \delta q_\alpha(\boldsymbol{r})\, \mathcal{C}^\alpha(\mathbf{1},\mathbf{2},t;\boldsymbol{r})\,. \tag{3.69}$$

The index α refers to the different types of perturbations in the solar model, for example perturbations to sound speed or flows. The sum over α is over all relevant types of perturbations. We note that any particular perturbation δq_α may appear in both the operator $\delta\mathcal{L}$ and the perturbation to the source covariance $\delta\mathbf{M}$. For example a flow will both advect waves as well as Doppler shift the sources. For any particular $\delta\mathbf{M}(\delta q)$ it may be helpful to do partial integrations on equation (3.67) before making the change of variable $\boldsymbol{r} = (\boldsymbol{s}+\boldsymbol{s}')/2$ described above. In Section 3.4.2, we will show a detailed example of the derivation of $\mathcal{C}^\alpha$ for local perturbations to source strength and damping rate for surface gravity waves.

Earlier in this section we showed how to relate the travel-time perturbations $\delta\tau_\pm$ to the perturbation to the cross-correlation δC. Using equation (3.69) for δC, and equation (3.50) for $\delta\tau_\pm$, we obtain:

$$\delta\tau_\pm(\mathbf{1},\mathbf{2}) = \int_{\odot} \mathrm{d}\boldsymbol{r}\; \delta q_\alpha(\boldsymbol{r}) \int_{-\infty}^{\infty} \mathrm{d}t\; W_\pm(\mathbf{1},\mathbf{2},t)\, \mathcal{C}^\alpha(\mathbf{1},\mathbf{2},t;\boldsymbol{r})\,. \tag{3.70}$$

As we want to define sensitivity kernels in the form

$$\delta\tau_\pm(\mathbf{1},\mathbf{2}) = \int_{\odot} \mathrm{d}\boldsymbol{r}\; \delta q_\alpha(\boldsymbol{r})\, K^\alpha_\pm(\mathbf{1},\mathbf{2};\boldsymbol{r})\,, \tag{3.71}$$

we make the identification

$$K^\alpha_\pm(\mathbf{1},\mathbf{2};\boldsymbol{r}) = \int_{-\infty}^{\infty} \mathrm{d}t\; W_\pm(\mathbf{1},\mathbf{2},t)\, \mathcal{C}^\alpha(\mathbf{1},\mathbf{2},t;\boldsymbol{r})\,. \tag{3.72}$$

By definition, $K^\alpha_\pm$ represent the local sensitivity of the travel-time perturbations $\delta\tau_\pm$ to perturbations to the model, δq_α. From the above equation we can see that the kernels depend on both the definition of travel time, through the functions $W_\pm$, as well as on the zero-order problem and the form of the first-order perturbations, through $\mathcal{C}^\alpha$. The inputs needed to compute $W_\pm$ are the zero-order cross-correlation

C^0, and the reference wavelet $C^{\rm ref}$ and window function $f(t)$ used in the travel-time measurement procedure (eq. [B.7]). The function $\mathcal{C}^\alpha$ depends on the source covariance, the Green's function, the filter, and the forms of the wave operator and the source function (eqs. [3.66] and [3.67]).

We have now shown a general procedure for computing travel-time kernels for any particular model. In order to demonstrate the utility and feasibility of this procedure we will, in the next section, derive two-dimensional kernels for surface gravity waves.

3.4.2 A Surface Gravity Wave Example

In this section we derive the sensitivity of surface gravity wave travel times to local perturbations to source strength and damping rate. We work in a plane-parallel model with constant density and gravity. In this model, wave excitation and attenuation act only at the fluid surface, and the problem can be reduced to a two-dimensional problem. Our model is a very simplified version of the actual solar f-mode case, yet incorporates most of the basic physics. We will follow the basic recipe outlined in Section 3.4.1 for deriving kernels.

The example is written in four parts. First we fully specify the problem: we derive the equations of motion, encapsulated in the operator $\mathcal{L}$, and describe our models for the source covariance and wave damping. We also describe the filter $\mathcal{F}$ which includes an approximation to the SOHO-MDI point spread function. After specifying the problem we then compute the zero-order solution to the problem: the Green's function, power spectrum, and zero-order cross-correlation. With the Green's function and cross-correlation in hand, we next derive travel-time kernels for perturbations in source strength and damping rate. We conclude with a comparison of distributed-source kernels and kernels obtained in the single-source picture.

Specification of the Problem

We consider a simple plane-parallel medium appropriate to studying waves with wavelengths small compared to the solar radius. The geometry is shown in Figure 3.10. The height coordinate is z, measured upward, and a horizontal coordinate vector is denoted by $\boldsymbol{x}$. Gravitational acceleration is assumed to be constant, $-g\hat{\boldsymbol{z}}$,

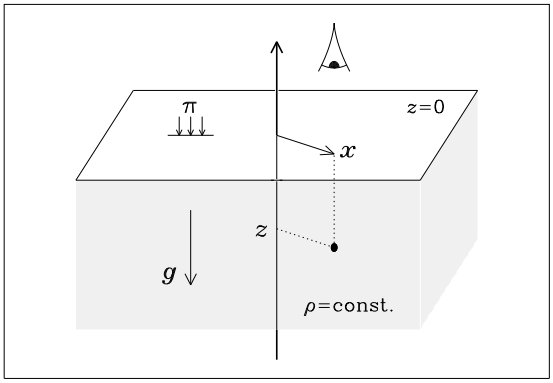

Figure 3.10: The basic setup for the example. The coordinate z denotes height and $\boldsymbol{x}$ is a horizontal coordinate vector. The half space $z < 0$ is filled with an incompressible fluid of density ρ and the space above is empty. The line-of-sight vector is $\hat{\boldsymbol{\ell}} = \hat{\boldsymbol{z}}$, i.e. the observer is looking straight down at the surface. Gravitational acceleration is constant and points in the $-\hat{\boldsymbol{z}}$ direction. Surface gravity waves are excited by a stochastic pressure distribution Π applied at the surface, $z = 0$.

where $g = 274$ m s^{-2} is the solar surface value. For $z < 0$ the fluid has a uniform constant density ρ. This assumption simplifies the problem considerably and does not affect the dispersion relation ($\omega^2 = gk$). In addition, acoustic waves are not present in this problem because the medium is incompressible. In the steady background state there is a free surface at $z = 0$. The background pressure distribution, $P(z)$, is hydrostatic, with $P = -\rho g z$.

In the following subsections, we develop the equations of motion, encapsulated in the operator $\mathcal{L}$, and describe our models for the source covariance and the wave damping operator. We also describe the filter $\mathcal{F}$ which includes an approximation to the SOHO-MDI point spread function. The measurement procedure is specified by choosing the reference wavelet and the window function.

Equations of Motion

We now derive the equations of motion, which we want in the form of equation (3.51). For an inviscid fluid of constant density, the linearized equations of conservation of

mass and momentum read

$$\boldsymbol{\nabla} \cdot \boldsymbol{v} = 0\,, \tag{3.73}$$

$$\rho \dot{\boldsymbol{v}} + \boldsymbol{\nabla} p = \mathbf{0}\,, \tag{3.74}$$

where p is the pressure perturbation associated with the waves. Provided that there exists a time at which the velocity field is irrotational, it will remain irrotational for all time. We may imagine a medium free of waves as a starting condition and subsequently switch on the pressure sources at some initial time in the distant past. As a result we assume that

$$\boldsymbol{\nabla} \times \boldsymbol{v} = \mathbf{0} \tag{3.75}$$

holds for all times.

In the Sun the wave excitation mechanism is near-surface turbulent convection, with various types of sources distributed with depth (e.g Nigam & Kosovichev, 1999; Kumar & Basu, 2000). Here, we excite surface gravity waves by applying a stochastic pressure source Π at the fluid surface. Thus, the wave pressure perturbation, p, satisfies the linearized dynamic boundary condition

$$p - \rho g \xi = \Pi\,, \quad \text{at } z = 0\,, \tag{3.76}$$

where ξ is the vertical displacement, which has time derivative equal to the vertical velocity at the surface.

In principle, turbulent convection is also responsible for damping f modes (e.g. Duvall et al., 1998). Turbulent convection can also modify the dispersion relation (Murawski & Roberts, 1993). Here, however, we use a phenomenological model for wave attenuation by including a dissipative term $\rho \Upsilon \boldsymbol{v}$ in the momentum equation at the surface. The operator Υ is a temporal convolution which reproduces the observed damping rates; it will be discussed in detail later in this section. At the surface, the momentum equation thus becomes:

$$\rho \dot{\boldsymbol{v}} + \boldsymbol{\nabla} p = -\rho \Upsilon \boldsymbol{v}\,, \quad \text{at } z = 0\,. \tag{3.77}$$

Eliminating p from equations (3.77) and (3.76), the surface boundary conditions

reduce to the equation

$$\partial_z \ddot{w} - g\boldsymbol{\nabla}_{\rm h}^2 w - \partial_t \boldsymbol{\nabla}_{\rm h} \cdot (\Upsilon \boldsymbol{u}) = \frac{1}{\rho}\boldsymbol{\nabla}_{\rm h}^2 \dot{\Pi}\,, \tag{3.78}$$

where $\boldsymbol{\nabla}_{\rm h}$ is the horizontal gradient and $\boldsymbol{u}$ and w are the horizontal and vertical components of the wave velocity,

$$\boldsymbol{v} = \boldsymbol{u} + w\ \hat{\boldsymbol{z}}\,. \tag{3.79}$$

We note that perturbations at the surface do not affect equations (3.73) and (3.75) for $z < 0$. As a result the effect of surface perturbations is contained entirely in equation (3.78). Therefore the problem is completely specified by equation (3.78) on the surface and the auxiliary equations $\boldsymbol{\nabla}\times\boldsymbol{v} = \boldsymbol{0}$ and $\boldsymbol{\nabla}\cdot\boldsymbol{v} = 0$ for $z < 0$. The problem is thus essentially two-dimensional, and equation (3.78) is the relevant equation to put in the form of equation (3.51). So we have

$$\begin{aligned} \mathcal{L}\boldsymbol{v} &= \partial_z \ddot{w} - g\boldsymbol{\nabla}_{\rm h}^2 w - \partial_t \boldsymbol{\nabla}_{\rm h} \cdot (\Upsilon \boldsymbol{u})\,, & (3.80)\\ S &= \frac{1}{\rho}\boldsymbol{\nabla}_{\rm h}^2 \dot{\Pi}\,. & (3.81) \end{aligned}$$

We notice that the source function S is scalar, unlike in the general theory (§ 3.4.1). Now that we have specified the operator $\mathcal{L}$ and the source function S it remains only to follow the recipe presented in the theory section.

The first part of the recipe is to write the zero-order problem and the first-order Born approximation. We consider two different types of perturbations to the background state: a change in the damping operator, $\delta\Upsilon$, and a change in the source function, δS. The zero-order problem is

$$\mathcal{L}^0 \boldsymbol{v}^0 = S^0\,, \tag{3.82}$$

where

$$\begin{aligned} \mathcal{L}^0 \boldsymbol{v}^0 &= \partial_z \ddot{w}^0 - g\boldsymbol{\nabla}_{\rm h}^2 w^0 + \partial_t \Upsilon^0 \partial_z w^0\,, & (3.83)\\ S^0 &= \frac{1}{\rho}\boldsymbol{\nabla}_{\rm h}^2 \dot{\Pi}^0\,. & (3.84) \end{aligned}$$

Here, S^0 is the zero-order source function, $\mathcal{L}^0$ the zero-order wave operator, and $\boldsymbol{v}^0$ the unperturbed wave velocity. We have used the fact that the zero-order damping operator Υ^0 commutes with spatial derivatives. The first-order approximation gives:

$$\mathcal{L}^0\,\delta\boldsymbol{v} = -\delta\mathcal{L}\,\boldsymbol{v}^0 + \delta S\,, \tag{3.85}$$

where

$$-\delta\mathcal{L}\,\boldsymbol{v}^0 = \partial_t \boldsymbol{\nabla}_{\mathrm{h}} \cdot (\delta\Upsilon\,\boldsymbol{u}^0)\,, \tag{3.86}$$

$$\delta S = \frac{1}{\rho}\boldsymbol{\nabla}^2_{\mathrm{h}}\,\delta\dot{\Pi}\,. \tag{3.87}$$

Here, δS is the perturbation to the source function, $\delta\mathcal{L}$ the perturbation to the wave operator, and $\delta\boldsymbol{v}$ the first Born approximation to the wave velocity. Notice that equation (3.85) has the same operator, $\mathcal{L}^0$, on the left-hand side as the zero-order problem (eq. [3.82]).

Source Covariance

In order to model the zero-order covariance M^0 of the source function S^0, which is necessary to compute the cross-correlation, we introduce the covariance of the applied surface pressure distribution Π^0,

$$\rho^2 m^0(\boldsymbol{x}, t; \boldsymbol{x}', t') = \mathrm{E}\left[\Pi^0(\boldsymbol{x}, t)\,\Pi^0(\boldsymbol{x}', t')\right], \tag{3.88}$$

which is a physical quantity. In terms of m^0, the zero-order source covariance M^0 is given by

$$M^0(\boldsymbol{x}, t; \boldsymbol{x}', t') = \boldsymbol{\nabla}^2_{\boldsymbol{x}}\,\boldsymbol{\nabla}^2_{\boldsymbol{x}'}\,\partial_t\,\partial_{t'}\,m^0(\boldsymbol{x}, t; \boldsymbol{x}', t')\,, \tag{3.89}$$

where $\boldsymbol{\nabla}^2_{\boldsymbol{x}}$ denotes the horizontal Laplacian with respect to the variable $\boldsymbol{x}$. Guided by the observations of Title et al. (1989) we write m^0 as a product of spatial and temporal decaying exponentials. Under the assumption of translation invariance (in time and space):

$$m^0(\boldsymbol{x}; t; \boldsymbol{x}', t') = a\,\frac{e^{-\|\boldsymbol{x}-\boldsymbol{x}'\|/L_{\mathrm{s}}}}{2\pi L_{\mathrm{s}}^2}\,\frac{e^{-|t-t'|/T_{\mathrm{s}}}}{2T_{\mathrm{s}}}\,. \tag{3.90}$$

Here $L_{\rm s}$ is the correlation length and $T_{\rm s}$ the correlation time of the lowest-order turbulent pressure field Π^0. The constant a is the overall amplitude of m^0. The normalization factors $2\pi L_{\rm s}^2$ and $2T_{\rm s}$ are included so that in the limits of $L_{\rm s} \to 0$ and $T_{\rm s} \to 0$, m^0 becomes the product of two Dirac delta functions, $\delta_{\rm D}(\boldsymbol{x} - \boldsymbol{x}')$ and $\delta_{\rm D}(t - t')$.

Title et al. (1989) computed the covariance function of quiet-sun granulation intensity and found exponential dependence on the temporal and spatial separations, $|t - t'|$ and $\|\boldsymbol{x} - \boldsymbol{x}'\|$, with correlation time 400 s and correlation length 450 km. For this work, we take $T_{\rm s} = 400$ s and $L_{\rm s} = 0$. Neglecting the source correlation length, i.e. treating the sources as spatially uncorrelated, is done for the sake of computational simplicity; it is not at all a limitation of the theory. The approximation of zero-correlation length is appropriate because L_s is smaller than a wavelength. For the form of m^0 given by equation (3.90), and the definition of the Fourier transform appropriate for functions that are translation invariant (eq. [C.4]), we obtain

$$m^0(\boldsymbol{k}, \omega) = \frac{a}{(2\pi)^3[1 + (\omega T_{\rm s})^2]}\,, \quad \text{as } L_{\rm s} \to 0\,, \tag{3.91}$$

which in particular does not depend on $\boldsymbol{k}$ for spatially uncorrelated sources. Here, as in the rest of the paper, $\boldsymbol{k}$ is the horizontal wave vector and ω is the angular frequency.

We now consider source perturbations. As we have already shown, what matters for the computation of cross-correlations is not the perturbation to the source but rather the perturbed source covariance, δM, which can be obtained from δm through

$$\delta M(\boldsymbol{x}, t; \boldsymbol{x}', t') \;=\; \boldsymbol{\nabla}_{\boldsymbol{x}}^2\, \boldsymbol{\nabla}_{\boldsymbol{x}'}^2\, \partial_t\, \partial_{t'}\, \delta m(\boldsymbol{x}, t; \boldsymbol{x}', t')\,. \tag{3.92}$$

Three possible types of perturbations to the source covariance are local changes in source correlation time, correlation length, and amplitude. For instance, Title et al. (1989) report different correlation times in quiet Sun and magnetic network. Magnetic fields affect near-surface convection and thus are expected to introduce local changes in the source strength as well. Here we consider only perturbations to the local amplitude, a, of m, i.e. to model regions of increased or decreased f-mode

emission. We choose

$$\delta m(\boldsymbol{x}, t; \boldsymbol{x}', t') = \frac{\delta a(\boldsymbol{r})}{a}\, m^0(\boldsymbol{x}, t; \boldsymbol{x}', t')\,, \tag{3.93}$$

with

$$\boldsymbol{r} = \frac{1}{2}(\boldsymbol{x} + \boldsymbol{x}')\,. \tag{3.94}$$

Here $\delta a(\boldsymbol{r})$ gives the local change in the amplitude of the source covariance. We have used the assumption that the source correlation length is small compared to the length scale of the spatial variation of the amplitude of the source function to write δa as a function of only the central position $\boldsymbol{r}$.

Damping

Theoretical descriptions of the damping of f modes by scattering from near-surface convective turbulence exist (e.g. Duvall et al., 1998), but we elect to use a phenomenological model for the sake of simplicity. It is known from observations that high-frequency waves are damped more strongly than low-frequency waves (e.g. Duvall et al., 1998). As a result we need a frequency-dependent damping rate. The easiest way to implement general frequency dependence is through a temporal convolution (e.g. Dahlen & Tromp, 1998). Thus, we express the zero-order damping operator, Υ^0, as

$$\Upsilon^0 \boldsymbol{v}(\boldsymbol{x}, t) = \frac{1}{2\pi} \int_{-\infty}^{\infty} \mathrm{d}t'\; \Gamma^0(t - t')\, \boldsymbol{v}(\boldsymbol{x}, t')\,. \tag{3.95}$$

We have assumed that damping is acting purely locally. A more sophisticated model would presumably include a spatial convolution in addition to the temporal convolution. With the Fourier convention given in Appendix C, Υ^0 can be written as

$$\Upsilon^0 \boldsymbol{v}(\boldsymbol{k}, \omega) = \Gamma^0(\omega)\, \boldsymbol{v}(\boldsymbol{k}, \omega)\,, \tag{3.96}$$

where $\Gamma^0(\omega)$ is the temporal Fourier transform of $\Gamma^0(t)$. In addition, we see that the operator $\partial_t + \Upsilon^0$, which appears in equation (3.77), becomes multiplication by $-\mathrm{i}\omega + \Gamma^0(\omega)$ in the Fourier domain.

For the sake of simplicity, we choose the function $\Gamma^0(t)$ to be real and even in time. As a result $\Gamma^0(\omega)$ is real and even. A non-physical consequence of this choice

is that the damping operator is not causal. We will see, however, that the Green's function derived using this damping operator is still causal. A treatment of causal frequency-dependent damping can be found in Dahlen & Tromp (1998). In order to damp all frequencies ω the function $\Gamma^0(\omega)$ must be positive (this will be discussed later in this chapter). We will see later in this section that $\Gamma^0(\omega)$ is the full frequency width at half maximum of the surface gravity wave power. We obtain a good fit to observed f-mode line widths (Duvall et al., 1998) if we write $\Gamma^0(\omega)$ in the form

$$\Gamma^0(\omega) = \gamma \left| \frac{\omega}{\omega_\star} \right|^\beta , \tag{3.97}$$

with the parameters $\omega_\star/2\pi = 3$ mHz , $\gamma/2\pi = 100$ μHz, and $\beta = 4.4$. This fit is accurate in the range $1.5\,\mathrm{mHz} < \omega/2\pi < 5\,\mathrm{mHz}$. The frequency dependence of the damping rate is strong.

There are two basic types of perturbations to the local damping rate: a change in the amplitude of the damping rate, γ, and a change in the exponent, β. In this chapter we only consider the former and write the perturbation to the damping operator as

$$\delta\Upsilon\, \boldsymbol{v}(\boldsymbol{x},t) = \frac{\delta\gamma(\boldsymbol{x})}{\gamma}\, \Upsilon^0 \boldsymbol{v}(\boldsymbol{x},t)\,, \tag{3.98}$$

where $\delta\gamma(\boldsymbol{x})/\gamma$ is the local fractional perturbation in the damping rate.

Observational Filter

For this example we take the line-of-sight vector to be vertical and independent of horizontal position, $\hat{\boldsymbol{\ell}} = \hat{\boldsymbol{z}}$. Then in accordance with equation (1.19) the observable is

$$\phi(\boldsymbol{x},t) = \mathcal{F}\{\boldsymbol{v}(\boldsymbol{x},t)\cdot\hat{\boldsymbol{z}}\}\,. \tag{3.99}$$

In this example we consider only the case where there is no spatial or temporal window function in the filter $\mathcal{F}$, i.e. we observe the wavefield over an area A and a time interval T which are both very large. Therefore the filter $\mathcal{F}$ can be represented by multiplication by a function $F(\boldsymbol{k},\omega)$ in the Fourier domain,

$$\phi(\boldsymbol{k},\omega) = F(\boldsymbol{k},\omega)\, w(\boldsymbol{k},\omega)\,, \tag{3.100}$$

where $w = \boldsymbol{v}\cdot\hat{\boldsymbol{z}}$. The function F includes the instrumental Optical Transfer Function (OTF), which is the Fourier transform of the point spread function of the telescope optics, as well as the effect of the finite pixel size of the detector. We use an azimuthal average of the OTF estimated by Tarbell et al. (1997) for the SOHO-MDI telescope in its high-resolution mode near disk center. We correct the OTF for the effect of finite pixel size, ϵ, by multiplying by $\mathrm{sinc}(k\epsilon/2)$, with $\epsilon = 0.83$ Mm and $k = \|\boldsymbol{k}\|$.

In general, F also includes the filter used to select the particular waves of interest in the k-ω diagram and to remove low frequency noise from the data. In this example there is only one ridge in the k-ω diagram, corresponding to surface gravity waves. We choose a filter which is zero for frequencies less than $\omega_{\min}/2\pi = 2$ mHz and more than $\omega_{\max}/2\pi = 4$ mHz, as was done for the data shown in Figure 1.1.

We include an additional factor, R, in the filter to make our unstratified example look more solar. The function $R(k)$ is the ratio of mode inertia in our model to mode inertia in a standard stratified solar model:

$$R(k) = \frac{\rho \int_{-\infty}^{0} e^{2kz}\,\mathrm{d}z}{\int_{-\infty}^{z_\star} \rho_\odot(z)\, e^{2kz}\,\mathrm{d}z}\,. \tag{3.101}$$

Here ρ is the constant density in our model and $\rho_\odot$ is the density as a function of height in the solar model. We use the solar model of Christensen-Dalsgaard et al. (1993) complemented by the chromospheric model of Vernazza et al. (1981) up to $z_\star = 2$ Mm. In the solar model $z = 0$ is the photosphere. If we had started from the full stratified solar problem we would presumably obtain a solar-like power spectrum without this correction factor.

To summarize, we take the filter F to be:

$$F(\boldsymbol{k},\omega) = \mathrm{OTF}(k)\, R(k)\, \mathrm{Hea}(\omega - \omega_{\min})\, \mathrm{Hea}(\omega_{\max} - \omega)\,, \tag{3.102}$$

where Hea is the Heaviside step function. The OTF and the k dependence of the full filter, F, are shown in Figure 3.11. We repeat that we have not included the effect of an observational time window, nor the effect of observing a finite area on the Sun. Both of these effects could be included, though the filter could no longer be represented as a simple multiplication in the Fourier domain.

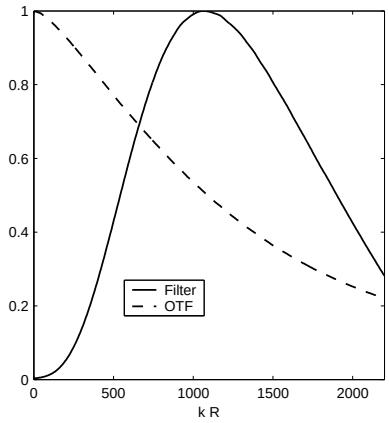

Figure 3.11: The wavenumber dependence of the filter F and of the OTF for the example calculation. The dashed line is the azimuthal average of the OTF estimated by Tarbell et al. (1997) for the SOHO-MDI high-resolution telescope. The filter F is the product of the OTF and the mode-mass correction R given by equation (3.101). Notice that the mode-mass correction suppresses the low-wavenumber part of the spectrum, which gives better agreement between our unstratified model and a stratified solar model, for which low wavenumbers modes are difficult to excite.

Measurement of Travel Times

As explained in section 3.4.1, the observer needs to select the reference wavelet $C^{\rm ref}$ and the window function f in order to make a travel-time measurement. For this example, we choose $C^{\rm ref}$ to be the zero-order cross-correlation of the model,

$$C^{\rm ref}(\mathbf{1},\mathbf{2},t) = C^0(\mathbf{1},\mathbf{2},t)\,, \tag{3.103}$$

and the window function f to be the Heaviside step function,

$$f(t) = \mathrm{Hea}(t)\,. \tag{3.104}$$

For this choice of reference wavelet, the zero-order travel times $\tau^0_\pm$ are zero (see Appendix B). The window function f is acceptable as we have only a single skip (surface waves). Using equation (B.9), we rewrite the travel-time perturbations $\delta\tau_\pm$

in terms of the temporal Fourier transforms of $W_\pm$ and δC:

$$\delta\tau_\pm(\mathbf{1},\mathbf{2}) = 4\pi \mathrm{Re} \int_0^\infty \mathrm{d}\omega\, W_\pm^*(\mathbf{1},\mathbf{2},\omega)\, \delta C(\mathbf{1},\mathbf{2},\omega)\,, \tag{3.105}$$

where Re selects the real part of the expression. The real and imaginary parts of $W_\pm(\omega)$ form a Hilbert transform pair:

$$W_\pm^*(\mathbf{1},\mathbf{2},\omega) = \frac{-\mathrm{Hilb}[\omega C^0(\mathbf{1},\mathbf{2},\omega)] \mp \mathrm{i}\omega C^0(\mathbf{1},\mathbf{2},\omega)}{4\pi \int_0^\infty \omega'^2 |C^0(\mathbf{1},\mathbf{2},\omega')|^2\, \mathrm{d}\omega'}\,, \tag{3.106}$$

where Hilb[·] denotes the Hilbert transform (Saff & Snider, 1993). Note that we used the fact that $C^0(t)$ is even, as will be shown later in this section. We now have an explicit definition of the travel-time perturbations $\delta\tau_+$ and $\delta\tau_-$ for our example.

The mean travel-time perturbation, $\delta\tau_{\mathrm{mean}}$, and the travel-time difference, $\delta\tau_{\mathrm{diff}}$, can be expressed in the form of equation (3.105) with weight functions $W^*_{\mathrm{mean}}(\omega)$ and $W^*_{\mathrm{diff}}(\omega)$ given by

$$W^*_{\mathrm{mean}} = \frac{1}{2}\left(W_+^* + W_-^*\right), \tag{3.107}$$

$$W^*_{\mathrm{diff}} = W_+^* - W_-^*\,. \tag{3.108}$$

From equation (3.106), and because $C^0(\omega)$ is real, we see that $W^*_{\mathrm{mean}}(\omega)$ is real and that $W^*_{\mathrm{diff}}(\omega)$ is imaginary. Thus the real part of the perturbation to the cross-correlation, $\delta C(\omega)$, introduces a mean travel-time perturbation. The imaginary part of $\delta C(\omega)$ causes a travel-time difference.

Zero-Order Solution

Now that the problem has been fully specified, we can compute the Green's function, the power spectrum, and the cross-correlation for the zero-order model. We show that the power spectrum in our example resembles the solar f-mode spectrum. We find that the unperturbed cross-correlation is the inverse Fourier transform of the power spectrum.

Green's Function

Here we derive the Green's function appropriate for solving a problem of the form of equation (3.82). The vector Green's function, $\boldsymbol{G}(\boldsymbol{x}, z, t; \boldsymbol{s}, t_{\rm s})$, is the velocity response at horizontal coordinate $\boldsymbol{x}$, height z, and time t to an impulsive source in S at surface location $\boldsymbol{s}$ and time $t_{\rm s}$. In our example S is scalar, so we need only one vector Green's function, and we drop the superscript on the Green's function, which appeared in the general theory (eq [3.56]). By definition $\boldsymbol{G}$ solves the surface boundary condition

$$\mathcal{L}^0 \boldsymbol{G}(\boldsymbol{x}, z, t; \boldsymbol{s}, t_{\rm s}) = \delta_{\rm D}(\boldsymbol{x} - \boldsymbol{s})\ \delta_{\rm D}(t - t_{\rm s}) \quad \text{at } z = 0, \tag{3.109}$$

with the additional constraints that $\boldsymbol{G}$ must be irrotational and divergenceless in the bulk, as well as vanish as $z \to -\infty$. The Green's function $\boldsymbol{G}$ is only a function of the horizontal spatial separation $\boldsymbol{x} - \boldsymbol{s}$, the time lag $t - t_{\rm s}$, and the observation height z. Using the Fourier convention given by equation (C.4), the Fourier transform of the Green's function can be written

$$\boldsymbol{G}(\boldsymbol{k}, \omega; z) = \frac{(\mathrm{i}\hat{\boldsymbol{k}} + \hat{\boldsymbol{z}})\ e^{kz}}{(2\pi)^3 k\,[gk - \omega^2 - i\omega\Gamma^0(\omega)]}\,, \tag{3.110}$$

where $\hat{\boldsymbol{k}} = \boldsymbol{k}/k$. We remind the reader that in this example the wave vector $\boldsymbol{k}$ is horizontal. From the above expression we can see that the horizontal component of $\boldsymbol{G}(\boldsymbol{k}, \omega; z)$ is in the direction of $\boldsymbol{k}$ and that the horizontal and vertical components are of the same magnitude and $\pi/2$ out of phase. The amplitude of the Green's function decays exponentially with depth; the same result would apply for a vertically stratified medium (Lamb, 1932). At fixed wavenumber k, the Green's function has resonant frequencies $\omega \simeq \pm\sqrt{gk} - \mathrm{i}\Gamma^0/2$ in the limit of small damping. We recognize the dispersion relation for deep water waves. Since $\Gamma^0(\omega)$ is positive, the imaginary part of the two poles of the Green's function is negative. This ensures that the Green's function is causal (e.g. Saff & Snider, 1993). For later use, we also introduce another Green's function,

$$\mathcal{G}^{\Pi}(\boldsymbol{k}, \omega) = \mathrm{i}\omega k^2 F(\boldsymbol{k}, \omega) G_z(\boldsymbol{k}, \omega, z = 0)\,, \tag{3.111}$$

which gives the vertical velocity at the surface resulting from an impulsive source in Π/ρ. The Green's function G_z is the $\hat{\boldsymbol{z}}$ component of $\boldsymbol{G}$ given by equation (3.110).

Power

By definition the power spectrum is the square of the modulus of the Fourier transform of the observable. For convenience, we consider the zero-order power spectrum per unit area and per unit time:

$$P(\boldsymbol{k},\omega) = \frac{(2\pi)^3}{AT}\mathrm{E}\left[|\phi^0(\boldsymbol{k},\omega)|^2\right] , \tag{3.112}$$

where A is the area and T the time interval over which the power is computed. After a few simple manipulations, we find that P is given by

$$P(\boldsymbol{k},\omega) = (2\pi)^6 \, |\mathcal{G}^{\Pi}(\boldsymbol{k},\omega)|^2 \, m^0(\boldsymbol{k},\omega) \, . \tag{3.113}$$

None of the terms in the above equation depend on the direction of $\boldsymbol{k}$. In particular, $m^0 = m^0(k,\omega)$ because the sources are spatially homogeneous and isotropic in the zero-order problem. In addition the filter F is a function only of the wavenumber k and frequency ω. Therefore the power spectrum is independent of the direction of $\boldsymbol{k}$. The term $|\mathcal{G}^{\Pi}(\boldsymbol{k},\omega)|^2$ specifies the shape of the resonance peaks in the power spectrum. For ω near $\sqrt{gk}$ we have approximately

$$P(\boldsymbol{k},\omega) \sim \frac{k^2F^2m^0}{4}\left[\left(\omega - \sqrt{gk}\right)^2 + \left(\Gamma^0/2\right)^2\right]^{-1} . \tag{3.114}$$

Thus, at fixed wavenumber, the line shape is Lorentzian with full-width at half-maximum $\Gamma^0(\omega)$.

Figure 3.12 compares the power spectrum for our model, $P(k,\omega)$, with the power spectrum for the solar f-mode ridge observed with the SOHO-MDI high-resolution telescope. The distribution of power with frequency and wavenumber confirms that there is a good agreement between the model and the observations.

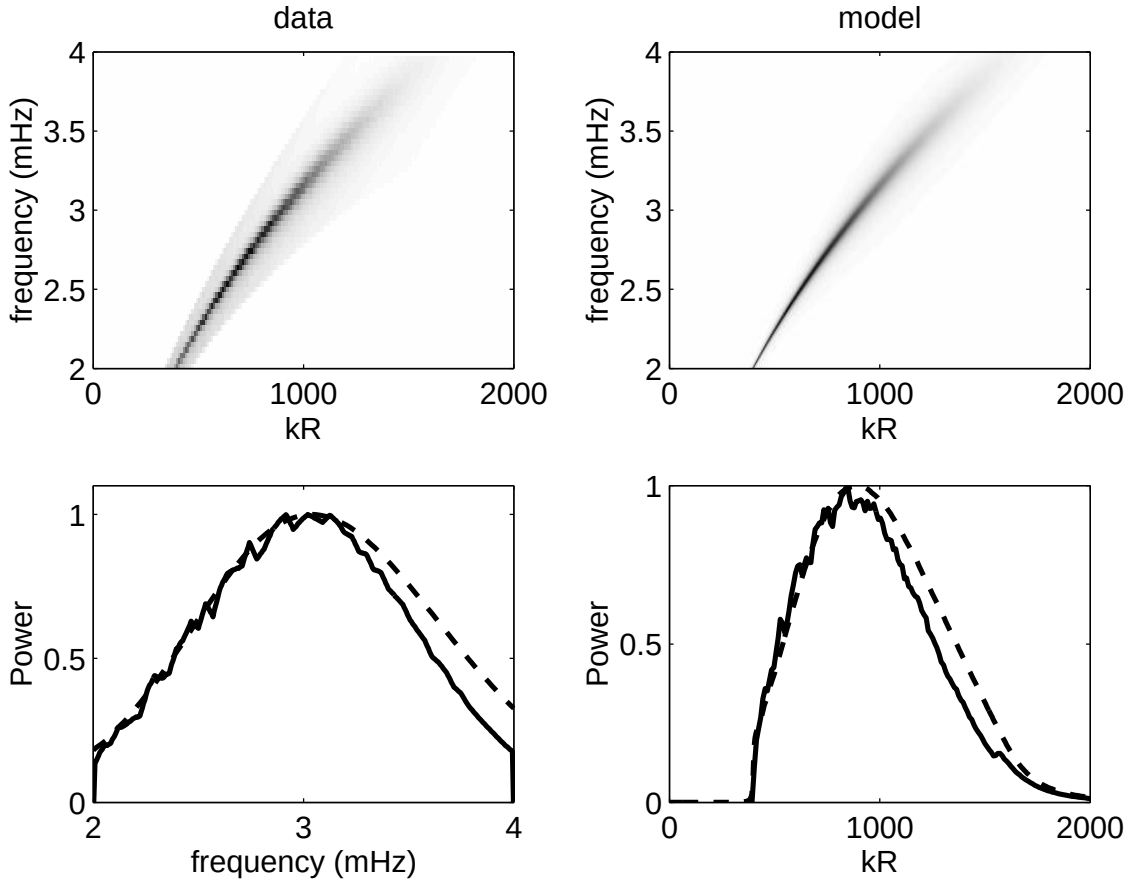

Figure 3.12: A comparison of observed and model power spectra. The upper-right figure shows the zero-order power spectrum in our model, $P(k,\omega)$, defined by equation (3.113). The coordinates are frequency, $\omega/2\pi$, and dimensionless wavenumber, $kR_\odot$, where $R_\odot = 696$ Mm is the solar radius. In the upper-left figure is the azimuthal average of the power observed with the SOHO-MDI high-resolution telescope. The f-mode ridge has been isolated by a simple boxcar filter. The lower-left panel displays the power integrated over wavenumber, as a function of frequency. The dashed and solid lines refer to the model and the observations respectively. The lower-right figure shows the power integrated over frequency, as a function of wavenumber $kR_\odot$. Again the dashed line refers to the model and the solid line to the data. In our model the source correlation length and time are $L_{\rm s} = 0$ and $T_{\rm s} = 400$ s. The agreement between the model and the observations could be further improved by considering a non-zero source correlation length, which would reduce the power at high spatial frequencies.

Cross-correlation

To obtain the zero-order cross-correlation, we use the definition of C^0 (eq. [3.62]), the expression for the source covariance (eq. [3.89]), and the definition of the Fourier transform to obtain:

$$C^0(\mathbf{1},\mathbf{2},t) = \iint_{-\infty}^{\infty} \mathrm{d}\boldsymbol{k} \int_{-\infty}^{\infty} \mathrm{d}\omega \; e^{\mathrm{i}\boldsymbol{k}\cdot\boldsymbol{\Delta}-\mathrm{i}\omega t} \; P(\boldsymbol{k},\omega)\,, \tag{3.115}$$

where $\boldsymbol{\Delta} = \mathbf{2} - \mathbf{1}$. For the zero-order problem the cross-correlation is therefore the inverse Fourier transform of the power spectrum. This is a consequence of the fact that the problem is translation invariant. Since in our example P does not depend on the direction of $\boldsymbol{k}$ we can perform the integration over the angle between $\boldsymbol{k}$ and $\boldsymbol{\Delta}$ to obtain

$$C^0(\mathbf{1},\mathbf{2},t) = 2\pi \int_0^{\infty} k\,\mathrm{d}k \int_{-\infty}^{\infty} \mathrm{d}\omega \; e^{-\mathrm{i}\omega t} J_0(k\Delta) P(k,\omega)\,, \tag{3.116}$$

where J_0 is the cylindrical Bessel function of order zero. From the above expression it is clear that the zero-order cross-correlation is only a function of the time lag t and the spatial separation between $\mathbf{1}$ and $\mathbf{2}$, $\Delta = \|\boldsymbol{\Delta}\|$. Notice that the amplitude of the cross-correlation falls off like $\Delta^{-1/2}$ at large distances as a result of the asymptotic form of $J_0(k\Delta)$. This factor accounts for the geometrical spreading of two-dimensional waves, like surface-gravity waves.

From the power spectrum, we can numerically compute the cross-correlation using equation (3.116). Figure 1.1 provides a comparison between the model cross-correlation C^0 (right panel) and an observed, from MDI-SOHO data, cross-correlation for the f-mode (left panel). The two cross-correlations show the same features, even at very short distances. The two branches of the cross-correlation correspond to the propagation of the energy of wave packets at the group speed, $v_{\mathrm{g}} = g/2\omega$, where ω is the central frequency. For a central frequency of 3 mHz the group speed is 7.3 km s^{-1}. The effect of dispersion is also clearly visible; the oscillating fine structure has a different slope than the envelope slope, given by the phase speed $v_{\mathrm{p}} = 2v_{\mathrm{g}}$. Low-frequency waves propagate faster than high-frequency waves, because the phase speed is inversely proportional to ω. Note that for distances less than about half a wavelength (2.5 Mm) the two branches of the cross-correlation are merged. This

implies that travel-time measurements are difficult in the near field. The effect of damping is to strongly suppress high-frequency waves at large distances. Figure 3.8 shows a plot of the zero order cross-correlation, $C^0 = C^{\rm ref}$, at a distance $\Delta = 10$ Mm. As a consequence of the dependence of the phase speed on frequency (dispersion), the instantaneous frequency of the cross-correlation is seen to increase with time lag t.

Kernels for Source Strength and Damping Rate

In this section we derive travel-time kernels, $K^a_\pm$ and $K^\gamma_\pm$, for perturbations to local source strength and damping rate respectively. These kernels connect travel-time perturbations $\delta\tau_\pm$ to fractional perturbations to the model:

$$\delta\tau_\pm(\mathbf{1},\mathbf{2}) \;=\; \int_{(A)} \mathrm{d}\boldsymbol{r}\; \frac{\delta a(\boldsymbol{r})}{a}\, K^a_\pm(\mathbf{1},\mathbf{2};\boldsymbol{r}) + \int_{(A)} \mathrm{d}\boldsymbol{r}\; \frac{\delta\gamma(\boldsymbol{r})}{\gamma}\, K^\gamma_\pm(\mathbf{1},\mathbf{2};\boldsymbol{r})\,. \quad (3.117)$$

Here $\delta a(\boldsymbol{r})/a$ is the local fractional change in the source strength and $\delta\gamma(\boldsymbol{r})/\gamma$ the fractional change in damping rate. The two-dimensional integrals are taken over all points $\boldsymbol{r}$ on the surface $z = 0$, denoted by (A).

In Appendix D we give an explicit derivation of the sensitivity kernels $K^\gamma_\pm$ and $K^a_\pm$. We first compute the sensitivity of the cross-correlation to small local changes in a and γ (eqs. [D.2], [D.4] and [D.5]). We then relate changes in the cross-correlation to changes in travel times, through the weight functions $W_\pm$ (eq. [3.70]). Because of the assumptions that we have made in this example, the kernels can be written in terms of separate one-dimensional integrals over horizontal wavenumber. In Appendix D we show that $K^a_\pm$ are given by

$$K^a_\pm(\mathbf{1},\mathbf{2};\boldsymbol{r}) \;=\; 4\pi\,\mathrm{Re}\int_0^\infty \mathrm{d}\omega\; W^*_\pm(\mathbf{1},\mathbf{2},\omega)\, m^0(\omega)\mathrm{I}^*(\Delta_1,\omega)\mathrm{I}(\Delta_2,\omega)\,, \quad (3.118)$$

where the integral $\mathrm{I}(d,\omega)$ is a function of a distance d and frequency ω only:

$$\mathrm{I}(d,\omega) = (2\pi)^3 \int_0^\infty k\,\mathrm{d}k\; J_0(kd)\mathcal{G}^{\mathbf{n}}(k,\omega)\,. \quad (3.119)$$

In equation (3.118), Δ_1 is the distance from $\mathbf{1}$ to $\boldsymbol{r}$ and Δ_2 is the distance from $\mathbf{2}$

to $\boldsymbol{r}$. The complex integral $\mathrm{I}(d,\omega)/(2\pi)^2$ is the spatial inverse Fourier transform of the Green's function $\mathcal{G}^{\mathbf{n}}(\boldsymbol{k},\omega)$.

As shown in Appendix D, the damping kernels $K^{\gamma}_{\pm}$ can also be written as combinations of two one-dimensional integrals, $\mathbb{I}(d,\omega)$ and $\mathbb{III}(d,\omega)$:

$$\begin{aligned} K^{\gamma}_{\pm}(\mathbf{1},\mathbf{2};\boldsymbol{r}) &= 4\pi(\hat{\boldsymbol{\Delta}}_1\cdot\hat{\boldsymbol{\Delta}}_2)\,\mathrm{Re}\int_0^{\infty}\mathrm{d}\omega\; W^{*}_{\pm}(\mathbf{1},\mathbf{2},\omega) \\ &\quad\times m^0(\omega)\;[\mathbb{I}(\Delta_1,\omega)\mathbb{III}(\Delta_2,\omega) \\ &\quad+\mathbb{I}(\Delta_2,\omega)\mathbb{III}^{*}(\Delta_1,\omega)]\,, \end{aligned} \tag{3.120}$$

where $\hat{\boldsymbol{\Delta}}_1$ is a unit vector in the direction $\boldsymbol{r}-\mathbf{1}$ and $\hat{\boldsymbol{\Delta}}_2$ is a unit vector in the direction $\boldsymbol{r}-\mathbf{2}$. The explicit forms of $\mathbb{I}$ and $\mathbb{III}$ are given in Appendix D. The function $\mathbb{III}$ is complex and involves only one Green's function, $\mathcal{G}^{\mathbf{n}}$. The real integral $\mathbb{I}$ involves two Green's functions, G_z and $\mathcal{G}^{\mathbf{n}}$, and is related to the scattering process (see Fig. 3.9).

We computed the kernels numerically, with grid spacings of 7×10^{-3} rad Mm^{-1} in k and 10^{-2} mHz in $\omega/2\pi$, which were selected so that the smallest line widths (1.5×10^{-2} rad Mm^{-1}, 1.7×10^{-2} mHz) would be resolved. We ran a second set of calculations at twice the above stated resolutions and saw only very minor changes in the resulting kernels.

Figures 3.13a and 3.13b show the kernels $K^{a}_{+}(\mathbf{1},\mathbf{2};\boldsymbol{r})$ and $K^{\gamma}_{+}(\mathbf{1},\mathbf{2};\boldsymbol{r})$ for the distance $\Delta=10$ Mm, as functions of horizontal position $\boldsymbol{r}=(x,y)$. The observation points $\mathbf{1}$ and $\mathbf{2}$ have coordinates $(x_1,y_1)=(-5,0)$ Mm and $(x_2,y_2)=(5,0)$ Mm respectively. An important observation is that the kernels K^{a}_{+} and K^{γ}_{+} are quite different; one does not simply have the opposite sign of the other. This means that a decrease in source strength is not equivalent to an increase in damping rate, as one might naively expect. In particular, the total integral of the source kernel is zero while the total integral of the damping kernel is positive, with a value of 5.9 s. A uniform increase in source strength results only in a change in the overall amplitude of the power spectrum (and thus in the cross-correlation) and as a result does not affect the travel time. In contrast, a uniform increase in the damping rate affects the shape of the power spectrum, and thus causes a travel-time perturbation $\delta\tau_{+}$. The kernels $K^{a,\gamma}_{+}$ have largest amplitude in the vicinity of the observation points

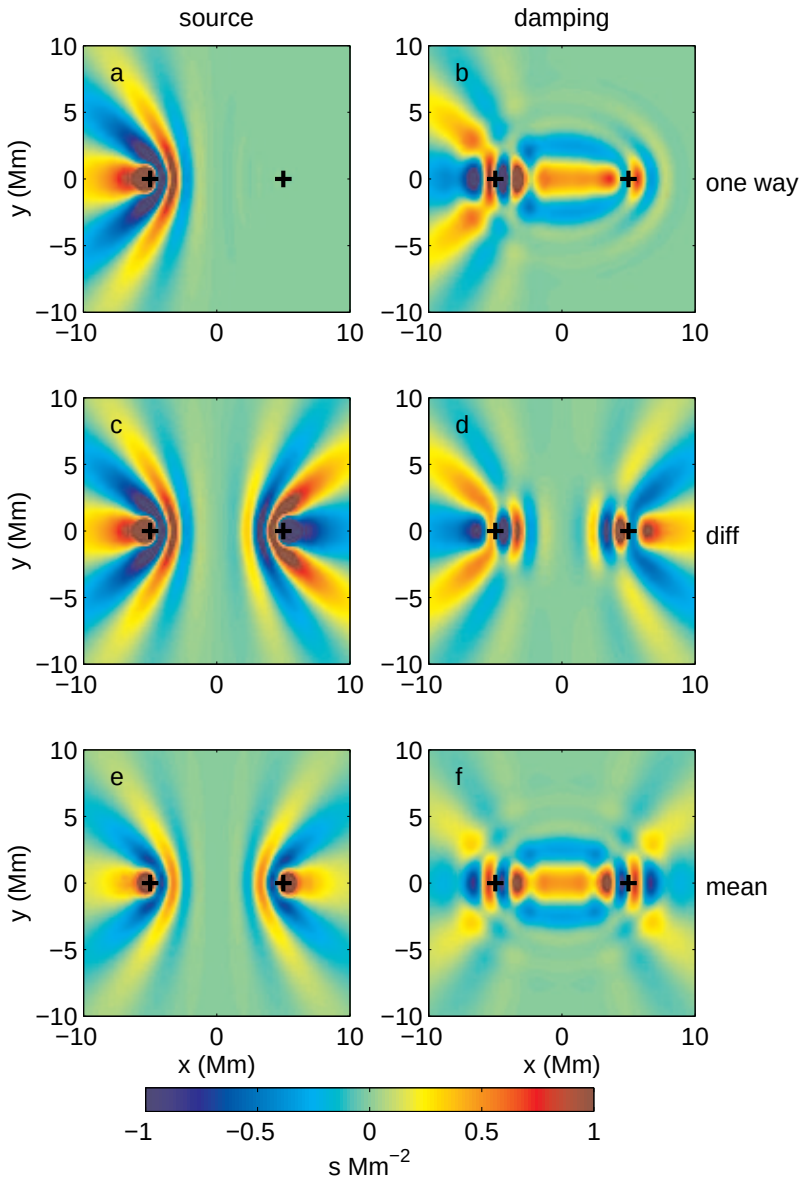

Figure 3.13: Travel-time sensitivity kernels for perturbations in source strength and damping rate as functions of position $\boldsymbol{r} = (x, y)$. The left column displays kernels for source strength, K^a, and the right column displays kernels for damping rate, K^γ. The top row gives the one-way travel-time kernels $K_+^{a,\gamma}$, the middle row gives the travel-time difference kernels $K_{\rm diff}^{a,\gamma}$, and the bottom row gives the mean travel-time kernels $K_{\rm mean}^{a,\gamma}$. The observation points **1** and **2** have the coordinates $(x_1, y_1) = (-5, 0)$ Mm and $(x_2, y_2) = (5, 0)$ Mm respectively, and are denoted by the black crosses in each panel. The color scale indicates the local value of the kernel, with blue representing negative values and red positive. The color scale is truncated at ± 1 s Mm^{-2}. The grid spacing is 0.14 Mm.

1 and **2**. Both K_+^γ and K_+^a have roughly the same magnitude, of the order a few $\mathrm{s\,Mm^{-2}}$. Both of the kernels oscillate spatially; this is a finite wavelength effect.

Hyperbola shaped features (with $\Delta_2 - \Delta_1 = \text{const}$) are present in both K_+^γ and K_+^a. As Woodard (1997) noted, all of the sources located along a particular hyperbola (with foci at the observation points) give a similar contribution to the cross-correlation, which explains the appearance of the kernel K_+^a. We emphasize that the kernel $K_+^a(\mathbf{1}, \mathbf{2}; \boldsymbol{r})$ is for the one-way travel time $\delta\tau_+(\mathbf{1}, \mathbf{2})$ which relates to waves moving from **1** to **2**. As a result only perturbations to the sources which produce waves moving from **1** to **2** can introduce a perturbation in $\tau_+(\mathbf{1}, \mathbf{2})$. This is clear from Figure 3.13a; the kernel K_+^a is only significant in the region, $x < 0$, which produces waves that arrive at **1** before they arrive at **2**.

The damping kernel K_+^γ is more complicated, as it shows ellipses ($\Delta_2 + \Delta_1 = \text{const}$) in addition to hyperbolas and results from scattering, unlike the source strength kernel. The ellipses are due to waves that go through **1**, scatter at $\boldsymbol{r}$, and are then observed at **2**. The hyperbolas correspond to scattered waves which arrive at **1** before the direct waves arrive at **2**. These two distinct processes will be discussed in more detail in Figure 3.17. Note that the damping kernels K^γ change sign on the circle $\hat{\boldsymbol{\Delta}}_1 \cdot \hat{\boldsymbol{\Delta}}_2 = 0$ which goes through **1** and **2**. This is a result of the details of the scattering of waves by local inhomogeneities in damping rate. The scattered wave depends on the direction of the incoming wave; back-scattered waves are in anti-phase with forward-scattered waves.

In this example, because $C^{\text{ref}} = C^0$ is even in time, $\delta\tau_-(\mathbf{1}, \mathbf{2}) = \delta\tau_+(\mathbf{2}, \mathbf{1})$. As a result the kernels K_-, for the travel-time perturbation $\delta\tau_-$, can be obtained from

$$K_-(\mathbf{1}, \mathbf{2}; \boldsymbol{r}) = K_+(\mathbf{2}, \mathbf{1}; \boldsymbol{r})\,. \tag{3.121}$$

This is not, however, a general rule; it depends on the choice of reference wavelet. The kernels for the perturbations to the travel-time mean and difference can be easily obtained from the kernels for the one-way travel times:

$$K^{a,\gamma}_{\text{mean}} = \frac{1}{2}(K_+^{a,\gamma} + K_-^{a,\gamma})\,, \tag{3.122}$$

$$K^{a,\gamma}_{\text{diff}} = K_+^{a,\gamma} - K_-^{a,\gamma}\,. \tag{3.123}$$

The kernels $K^{a,\gamma}_{\rm mean}$ and $K^{a,\gamma}_{\rm diff}$ are plotted in the remaining panels of Figure 3.13.

The kernels for the mean travel time are symmetric on interchange of **1** and **2** and the travel-time difference kernels are antisymmetric on interchange of **1** and **2**. Notice that like the one-way travel-time kernels, the kernels $K^{a,\gamma}_{\rm diff}$ and $K^{a,\gamma}_{\rm mean}$ are largest near the observation points **1** and **2**. We note that $K^{a}_{\rm diff}$ is roughly of the opposite sign from $K^{\gamma}_{\rm diff}$, except for inside the circle defined by $\hat{\mathbf{\Delta}}_1 \cdot \hat{\mathbf{\Delta}}_2 = 0$, where the sign is the same. A localized perturbation to source strength (damping rate) on the line $y = 0$ with $x \lesssim x_1$ gives an increase (decrease) in the travel-time difference.

In order to show the full range of variation of the kernels we plot, in Figure 3.14, cuts of the kernels $K^{a,\gamma}_{+}$ along the lines $y = 0$ and $x = 0$. Figure 3.14a shows that the source kernel is zero along the line $x = 0$, while the damping kernel is positive and maximum at $y = 0$. The side lobes (the second Fresnel zone) of K^{γ}_{+} extend out to 3.5 Mm. The slice along the line $y = 0$, Figure 3.14b, shows the complicated behavior of the kernels near the observation points, where they oscillate.

We have studied single-frequency kernels and seen that there is constructive interference between different frequency components along the line $y = 0, -\infty < x < x_2$ for K^{γ}_{+}, and the line $y = 0, -\infty < x < x_1$ for K^{a}_{+}. In the limit of infinite bandwidth, the kernels K^{γ}_{+} and K^{a}_{+} reduce to these rays respectively. This is in contrast with conventional ray theory where the ray is restricted to the line segment $y = 0, x_1 < x < x_2$.

In the past, travel-time kernels have been calculated in the "single-source picture" (Birch & Kosovichev, 2000; Jensen et al., 2000). In the following section we test the single-source method by comparing single-source kernels with the kernels calculated using a random distributed source model.

The Single Source Picture

The single-source picture consists of placing a single causal source at **1** and observing the effect of local perturbations on the wavefield observed at **2**. The one-way travel-time perturbation is approximated by the travel-time shift,

$$\delta\tau^{\rm ss}_{+}(\mathbf{1},\mathbf{2}) = -\frac{\int_{-\infty}^{\infty} {\rm d}t\ \delta\phi(\mathbf{2},t)\,\dot{\phi}^{0}(\mathbf{2},t)}{\int_{-\infty}^{\infty} {\rm d}t\ [\dot{\phi}^{0}(\mathbf{2},t)]^2}\,, \tag{3.124}$$

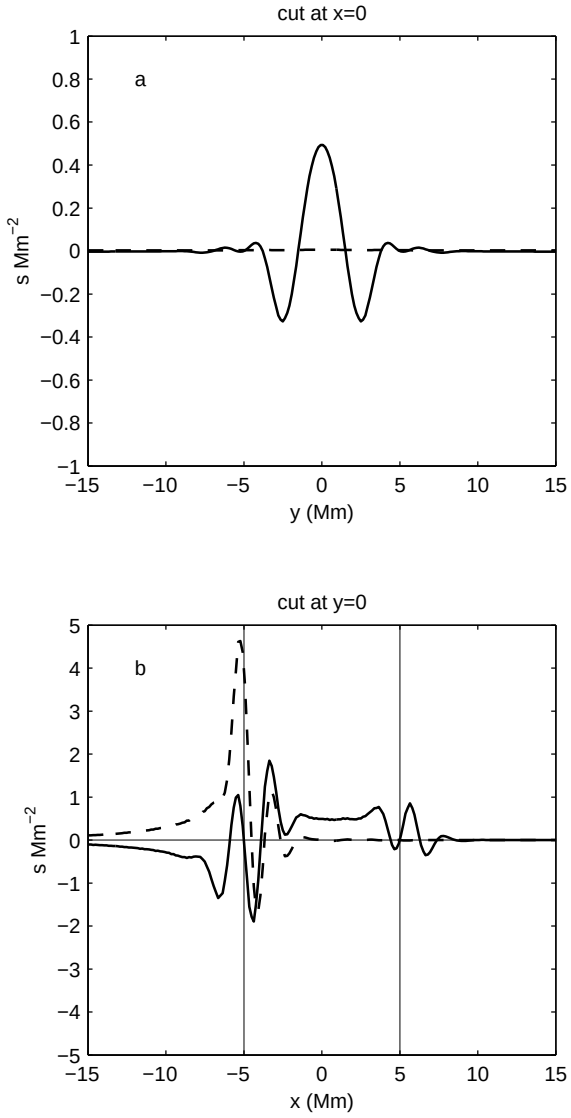

Figure 3.14: Cuts through the source and damping kernels, K_+^a and K_+^γ. Panel (a) shows cuts along the line $x = 0$ and panel (b) shows cuts along the line $y = 0$. The dashed line is for the source kernel K_+^a and the solid line is for the damping kernel K_+^γ.

between the unperturbed and perturbed signals at **2** (Birch et al., 2001a). This new definition of travel time is necessary; in the single-source picture there is no cross-correlation and thus our earlier definition of travel time can not be used. In equation (3.124), $\phi^0(\mathbf{2})$ and $\delta\phi(\mathbf{2})$ are the unperturbed and perturbed wavefields at **2**. The wavefield is generated by a causal pressure source placed at **1**:

$$\Pi(\boldsymbol{s}, t_{\rm s}) = \rho\,\Theta(\boldsymbol{s} - \mathbf{1}, t_{\rm s})\,. \tag{3.125}$$

The function Θ characterizes the pressure source and will later be used to tune the source spectrum.

In this section we consider the kernel $K_+^{\gamma,\rm ss}$, derived in the single-source picture, which gives the sensitivity of the travel-time perturbation $\delta\tau_+$ to a local fractional perturbation in the damping rate. The single-source picture cannot easily be used to derive a kernel for a source perturbation, which does not involve a scattering process.

By definition the kernel $K_+^{\gamma,\rm ss}$, which we derive in Appendix E, satisfies

$$\delta\tau_+^{\rm ss}(\mathbf{1},\mathbf{2}) = \int_{(A)} \mathrm{d}\boldsymbol{r}\; \frac{\delta\gamma(\boldsymbol{r})}{\gamma}\; K_+^{\gamma,\rm ss}(\mathbf{1},\mathbf{2};\boldsymbol{r})\,. \tag{3.126}$$

The definition of travel time given in equation (3.124) closely resembles the definition of travel time used in the general theory (eqs [B.6] and [B.9]) if $\phi(\mathbf{2},t)$ looks like the positive time-lag branch of the zero-order cross-correlation from the random-source model (§ 3.4.2). This condition implies that the spectrum of the source, $\Theta(\boldsymbol{k},\omega)$, is given by equation (E.8).

Figure 3.15 is a comparison of the single-source kernel $K_+^{\gamma,\rm ss}$ with the distributed-source kernel K_+^{γ}, computed in the previous section. The single-source kernel fails to reproduce the hyperbola shaped features that are seen in the random-source kernel, even though the ellipses can be seen in both (with the same order of magnitude and sign). A single causal source at **1** is not sufficient to generate all of the waves which are relevant to the problem of computing travel-time kernels (see Fig. 3.17).

Cuts at $y = 0$ through $K_+^{\gamma,\rm ss}$ and K_+^{γ} are shown in Figure 3.16, again for the distance $\Delta = 10$ Mm which was used in all previous plots of kernels. The kernels agree well for $x \gtrsim 0$, where the hyperbola shaped features in K_+^{γ} are absent. For

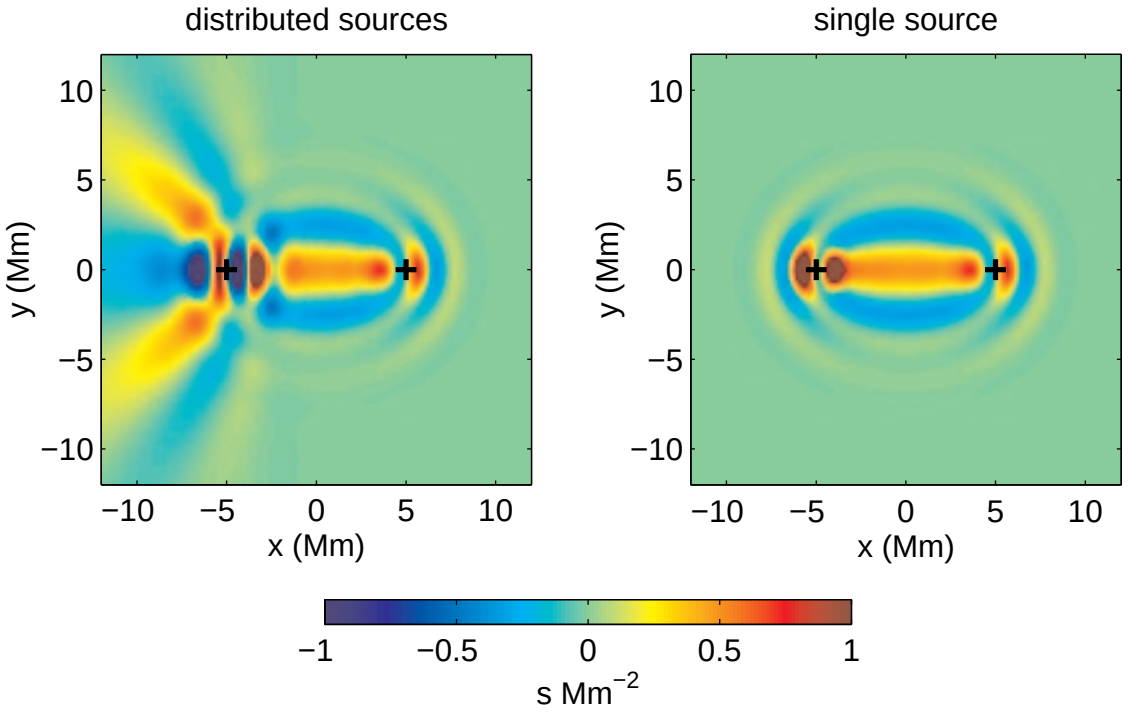

Figure 3.15: A comparison between single- and distributed-source kernels for damping rate. The left panel shows the distributed-source kernel for damping, K_+^γ (also shown in Fig. 3.13b). The right panel is the single-source kernel $K_+^{\gamma,\mathrm{ss}}$ discussed in this section and computed using equations (E.5) and (E.6). For the single-source kernel the source is located at **1** with coordinates $(-5, 0)$ Mm. The observation point **2** is located at $(0, 5)$ Mm.

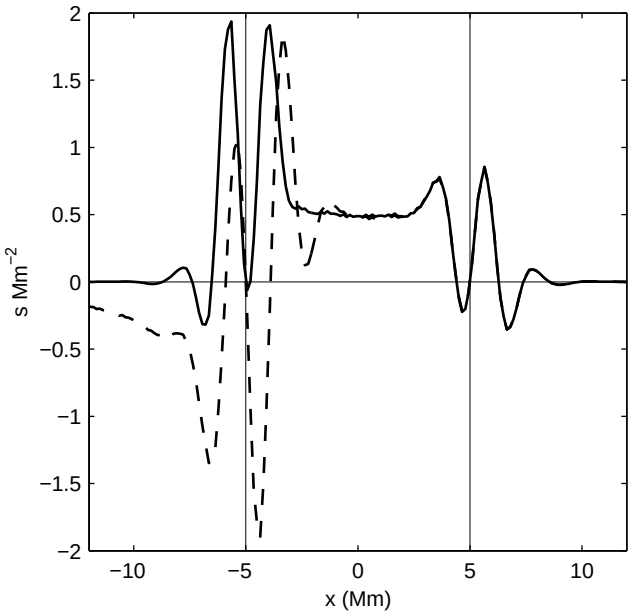

Figure 3.16: Cuts along the line $y = 0$ through the damping kernels K_+^γ and $K_+^{\gamma,\mathrm{ss}}$ shown in Figure 3.15. The dashed line is for the distributed-source kernel and the solid line is for the single-source kernel.

$x \lesssim 0$ the two kernels are quite different. In particular the single-source kernel is nearly zero for $x < -7$ Mm, while K_+^γ has a negative tail there.

In the limit of infinite bandwidth (ray theory), the single-source kernel $K_+^{\gamma,\mathrm{ss}}$ would be restricted to the line segment $y = 0$, $x_1 < x < x_2$. This is in contrast with our earlier finding that the distributed-source kernel K_+^γ would reduce to the ray $y = 0$, $-\infty < x < x_2$.

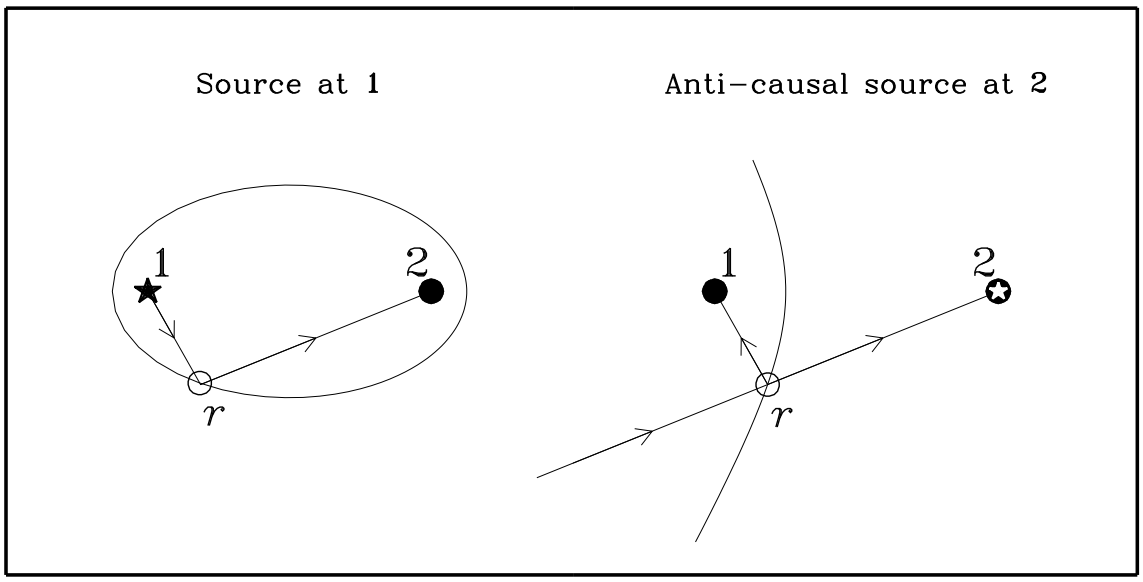

Figure 3.17: A graphical discussion of the single-source picture for computing kernels for the one-way travel time $\delta\tau_+(\mathbf{1},\mathbf{2})$. The left hand panel is the conventional single-source picture where a causal source is exploded at $\mathbf{1}$ and the scattered wave is observed at $\mathbf{2}$. The scattering point is denoted by $\boldsymbol{r}$. Perturbations located on curves with constant $\|\boldsymbol{r}-\mathbf{1}\|+\|\mathbf{2}-\boldsymbol{r}\|$ contribute to the scattered field with the same geometrical delay in travel time, and as a result ellipse shaped features are seen in the travel-time kernel. A single source at $\mathbf{1}$ does not, however, produce all of the waves which are relevant to computing correct travel-time kernels. The right-hand panel shows an example of a component to the wavefield which is missed in the single-source picture. An anti-causal source at $\mathbf{2}$ causes an incoming wave toward $\mathbf{2}$ which is then scattered at $\boldsymbol{r}$ and arrives at $\mathbf{1}$. For $\boldsymbol{r}$ near $\mathbf{1}$ this gives a signal that is first observed at $\mathbf{1}$ and then later at $\mathbf{2}$, i.e. looks like a wave moving from $\mathbf{1}$ to $\mathbf{2}$. Perturbations located on curves with constant $\|\boldsymbol{r}-\mathbf{1}\|-\|\mathbf{2}-\boldsymbol{r}\|$, i.e. hyperbolas, contribute to the scattered field with the same geometrical delay in travel time (Woodard, 1997). Were the single-source picture extended to include an anti-causal source at $\mathbf{2}$, hyperbola shaped features would be seen in the travel-time kernels. Note, however, that hyperbolas naturally appear in the distributed-source kernels $K_+^{a,\gamma}$ (Fig. 3.13a and 3.13b). The hyperbolas with $\|\boldsymbol{r}-\mathbf{1}\|-\|\mathbf{2}-\boldsymbol{r}\|>0$ are not seen as they do not affect the positive-time branch of the cross-correlation (the scattered wave arrives at $\mathbf{1}$ after the unperturbed wave arrives at $\mathbf{2}$).